https://doi.org/10.5194/egusphere-2022-1298
Preprint. Discussion started: 22 November 2022

Waves in SKRIPS: WaveWatch III coupling implementation and a case study of cyclone Mekunu

Rui Sun[1], Alison Cobb[1], Ana B. Villas Bôas[2], Sabique Langodan[3], Aneesh C. Subramanian[4], Matthew R. Mazloff[1], Bruce D. Cornuelle[1], Arthur J. Miller[1], Raju Pathak[3], and Ibrahim Hoteit[3]

[1]Scripps Institution of Oceanography, California, USA
[2]Department of Geophysics, Colorado School of Mines, Colorado, USA
[3]Physical Sciences and Engineering Division, King Abdullah University of Science and Technology (KAUST), Thuwal, Saudi Arabia
[4]Department of Atmospheric and Oceanic Sciences, University of Colorado Boulder, Colorado, USA

Correspondence: Rui Sun (rus043@ucsd.edu)

Abstract. In this work, we integrated the WaveWatch III model into the regional coupled model SKRIPS (Scripps–KAUST Regional Integrated Prediction System). The WaveWatch III model is implemented with flexibility, meaning the coupled system can run with or without the wave component. To demonstrate the impact of coupling we performed a case study using a series of coupled and uncoupled simulations of tropical cyclone Mekunu, which occurred in the Arabian Sea in May 2018. We examined the skill of the coupled model against the stand-alone WRF model and further investigated the impact of Langmuir turbulence in the coupled system. We found that the coupled model better captures the minimum pressure and maximum wind speed compared with the stand-alone WRF model. The characteristics of the tropical cyclone do not change significantly when using different options to parameterize the influence of waves on the ocean and the atmosphere. However, in the region of the cold wake, when Langmuir turbulence is considered in the coupled system, the sea surface temperature is about 0.5°C colder and the mixed layer is about 20 meters deeper. This indicates the ocean model is sensitive to the parameterization of Langmuir turbulence in the coupled simulations.

1 Introduction

Ocean surface waves play a key role in mediating exchanges of momentum, heat, and gases across the air–sea boundary (Fan et al., 2009; D'Asaro et al., 2014). The importance of surface waves in mediating air–sea interactions has been studied for decades (Fairall et al., 2003; Chen et al., 2007b). Surface waves can enhance upper ocean mixing through Langmuir turbulence, and neglecting the Langmuir mixing process may contribute to a shallow bias in mixed layer depth (MLD) (Li et al., 2016). In addition, waves determine the sea surface roughness, which affects wind stress that is important for short-term forecasting of tropical and sub-tropical cyclones (Olabarrieta et al., 2012).

Several regional coupled model studies have considered the effect of waves in air–sea interactions (e.g., Chen et al., 2007a; Warner et al., 2010; Liu et al., 2011; Wu et al., 2019; Lewis et al., 2019; Sauvage et al., 2022). Because of the importance of air–sea heat fluxes on the energy budget of a tropical cyclone (TC) (Emanuel, 1991), many of these studies have focused on TCs

https://doi.org/10.5194/egusphere-2022-1298
Preprint. Discussion started: 22 November 2022

and demonstrated increased accuracy in simulated intensity when coupled (e.g., Bender and Ginis, 2000; Chen et al., 2007b; Warner et al., 2010; Wu et al., 2019; Lewis et al., 2019; Li et al., 2022). Studies have also shown a strong coupled feedback in conditions where the heat content of the upper ocean layer is low, and a weak feedback when the ocean has a thick mixed layer (Mogensen et al., 2017). Saxby et al. (2021) highlight outstanding challenges, with high-resolution convection-permitting atmosphere-only and coupled configurations both accurately simulating TCs in the Bay of Bengal, suggesting that many of the deficiencies originate in the atmospheric model, but improvements could also be gained by coupling to a wave model.

The sea state is highly complex and variable in TC conditions, with Langmuir turbulence playing an important role in the upper-ocean mixing (Rabe et al., 2015; Reichl et al., 2016a, b). This turbulence is associated with coherent Langmuir circulation structures that exist and evolve over a range of spatial and temporal scales in the surface ocean (Langmuir, 1938; McWilliams et al., 1997; Thorpe, 2004). These structures arise through an interaction between ocean surface waves and the background Eulerian current. Langmuir turbulence enhances turbulent entrainment, deepening the mixed layer and leading to sea surface cooling, which in turn affects the air–sea heat fluxes that modulate the development of TCs. Studies of idealized TCs suggest including Langmuir turbulence in model simulations may cool the sea surface temperature (SST) by 0.5-0.7°C and increase the mixed layer depth by up to 20 m (Reichl et al., 2016b; Blair et al., 2017).

Because of the importance of ocean surface waves on air–sea interaction, we implemented a regional coupled ocean–wave–atmosphere model, with the capability of investigating the impact of surface waves on air–sea interaction (with emphasis on Langmuir turbulence). The goal of this work is twofold. First, we demonstrate the integration of the wave model WaveWatch III to the Scripps–KAUST Regional Integrated Prediction System (SKRIPS, Sun et al., 2019), which is a regional coupled ocean–atmosphere model that has been used to investigate extreme heat wave events on the shore of the Red Sea (Sun et al., 2019), North Pacific atmospheric rivers (Sun et al., 2021), and sea-ice evolution in the Antarctica (Cerovečki et al., 2022). The second goal is to evaluate the implementations of ocean surface waves in the coupled system. Here, we perform a series of coupled and uncoupled numerical simulations of tropical cyclone Mekunu in the Arabian Sea. Tropical cyclones in this region often lead to considerable destruction and loss of life due to inundations (Dube et al., 1997; Evan et al., 2011; Evan and Camargo, 2011). In addition, continued climate warming is expected to further amplify the risk of cyclones in the Arabian Sea and increase socio-economic implications for coastal communities in that region (Henderson-Sellers et al., 1998; Murakami et al., 2017; Bhatia et al., 2018). Cyclone Mekunu was the strongest tropical cyclone in the north Indian Ocean in 2018 (Government of India, 2018). It had a clear signature in SST cooling and MLD deepening, which can be used for testing the model. We investigate the sensitivities of the coupled model to the parameterizations of surface wave driven mixing to examine the effect of surface waves on air–sea interactions.

The rest of this paper is organized as follows. The implementation of the coupled model is described in Section 2. An overview of cyclone Mekunu, the design of the experiments, and the validation data are presented in Section 3. Section 4 details the numerical simulation results and Section 5 discusses the sensitivity of the simulation results to parameterizing Langmuir turbulence based on the evolving wave state. Section 6 concludes the paper with a summary of the main findings.

https://doi.org/10.5194/egusphere-2022-1298
Preprint. Discussion started: 22 November 2022

2 Methodology

2.1 Model Description

In this work, the version 6.07 (Tolman, 1991; WW3DG, 2019) of the WAVE-height, WATer depth and Current Hindcasting third generation wave model (WaveWatch III, hereinafter, WW3) is integrated into the SKRIPS model. The SKRIPS model (Sun et al., 2019) is a regional coupled ocean–atmosphere model: the oceanic model component is the MIT general circulation model (MITgcm) (Marshall et al., 1997; Campin et al., 2019) and the atmospheric model component is the Weather Research and Forecasting (WRF) model (Skamarock et al., 2019). The Earth System Modeling Framework (ESMF) (Hill et al., 2004) is used as the coupler to drive the coupled simulation. The National United Operational Prediction Capability (NUOPC) layer in the ESMF is used to simplify the implementations of component synchronization, execution, and other common tasks in the coupling (Hill et al., 2004).

Following our previous implementations (Sun et al., 2019) and the WW3–ESMF interface (WW3DG, 2019) for the prototype case, we implemented the WW3–ESMF interface in the coupled modeling system. We separated the WW3 main program into three subroutines that handle initialization, execution, and finalization. These subroutines are used by the ESMF/NUOPC coupler that controls the wave component in the coupled run. During the simulation, the surface boundary fields are exchanged via subroutine calls during the execution of the simulations by the WW3–ESMF interface. In addition, WW3 grid information is provided to the coupler in the initialization subroutine for online re-gridding of the exchanged boundary fields, although online regridding is not needed in the present work. To carry out the coupled simulation on HPC (high-performance computing) clusters, the WW3–ESMF interface runs in parallel via MPI (message passing interface) communications. We have also updated the MITgcm–ESMF and WRF–ESMF interfaces by including the inputs and outputs associated with the wave model. The wave component is implemented with flexibility, meaning the coupled system can run with or without the wave component.

The schematic description of the coupled model is shown in Fig. 1. In the coupling process, all model components send data to ESMF: MITgcm sends SST and ocean surface velocity; WRF sends surface atmosphere fields, including (1) net surface longwave and shortwave radiative fluxes, (2) surface latent and sensible heat fluxes, (3) 10-m wind speed, (4) precipitation, and (5) evaporation; WW3 sends the wave variables to ESMF, including the (1) bulk wave parameters (i.e., significant wave height, peak wavelength and mean wavenumber), (2) Surface Stokes drift, (3) momentum flux terms due to surface waves, and (4) Langmuir turbulence parameters. Then all model components read the data they need from ESMF: MITgcm reads surface atmospheric variables and wave variables; WRF reads the SST, ocean surface velocity, and wave variables; WW3 reads the wind speed and surface current velocity. The MITgcm model uses the surface atmospheric variables to prescribe surface forcing, including (1) total net surface heat flux, (2) surface wind stress, and (3) freshwater flux. The total net surface heat flux is computed by adding surface latent heat flux, sensible heat flux, net shortwave radiation flux, and net longwave radiation flux. The surface latent and sensible heat fluxes are computed using the COARE 3.0 bulk algorithm in WRF (Fairall et al., 2003).

https://doi.org/10.5194/egusphere-2022-1298
Preprint. Discussion started: 22 November 2022

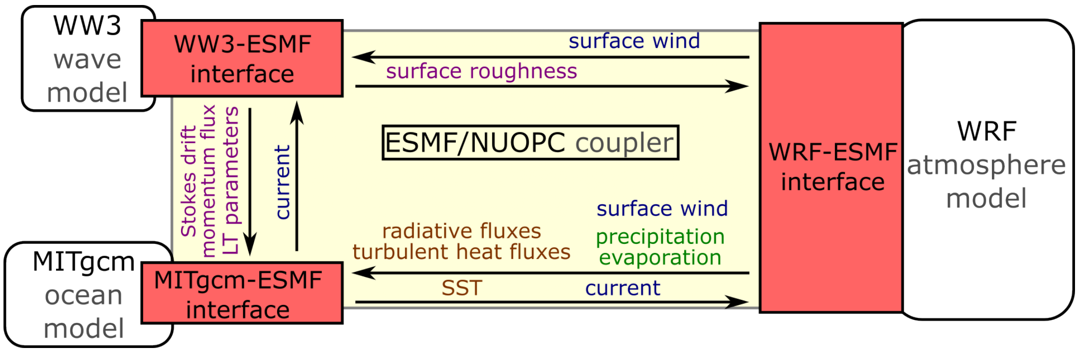

Figure 1. The schematic description of the SKRIPS regional coupled ocean–atmosphere model. The yellow block is the ESMF/NUOPC coupler; the white blocks are the ocean and atmosphere components; the red blocks are the implemented MITgcm–ESMF, WRF–ESMF, and WW3–ESMF interfaces.

2.2 Stokes Forces in MITgcm

The contribution of surface waves to the ocean momentum balance can be described by the wave-averaged momentum equations as follows (Suzuki and Fox-Kemper, 2016; Wu et al., 2019):

$$\frac{\mathrm{d}\boldsymbol{u}}{\mathrm{d}t} + (\boldsymbol{u}\cdot\nabla)\boldsymbol{u} = -\frac{1}{\rho_w}\nabla p + \boldsymbol{D}^u + \boldsymbol{b} - \boldsymbol{f}\times\boldsymbol{u} - \underbrace{(\boldsymbol{u^S}\cdot\nabla)\boldsymbol{u}}_{\text{Stokes advection}} - \underbrace{\boldsymbol{f}\times\boldsymbol{u^S}}_{\text{Stokes Coriolis}} - \underbrace{u_j^L\nabla u_j^S}_{\text{Stokes shear}}, \tag{1}$$

where t is time; $\nabla = (\partial x, \partial y, \partial z)$; ρ_w is the density of water; p is the pressure; $\boldsymbol{b} = -g\rho/\rho_w\hat{\boldsymbol{z}} = b\hat{\boldsymbol{z}}$ is the buoyancy term; $\hat{\boldsymbol{z}}$ is the vertical unit vector; $\boldsymbol{D^u}$ is the diffusion; $\boldsymbol{f} = f\hat{\boldsymbol{z}}$ is the Coriolis parameter; $-u_j^L\nabla u_j^S$ is the Stokes shear force; $\boldsymbol{u} = (u_1,u_2,u_3) = (u,v,w)$ is the wave-filtered Eulerian velocity (Eulerian velocity of the flow solved in MITgcm); $\boldsymbol{u^S}$ is the Stokes drift; $\boldsymbol{u^L} = \boldsymbol{u} + \boldsymbol{u^S}$ is the wave-filtered Lagrangian velocity. Here, the Einstein summation convention is used (e.g, $u_j^L\nabla u_j^S = u_1^L\nabla u_1^S + u_2^L\nabla u_2^S + u_3^L\nabla u_3^S$), although vector notation is used when it is unambiguous.

The tracer advection equation can be written as (Suzuki and Fox-Kemper, 2016; Wu et al., 2019):

$$\frac{\mathrm{d}c}{\mathrm{d}t} + (\boldsymbol{u}\cdot\nabla)c = -\underbrace{(\boldsymbol{u^S}\cdot\nabla)c}_{\text{Stokes advection}} + D^c, \tag{2}$$

where c is a scalar quantity, such as potential temperature and salinity; D^c is the diffusion.

The Stokes–Advection and Stokes–Coriolis terms are implemented in a straightforward way. The profiles of Stokes velocity are determined based on Breivik et al. (2014). Considering the effect of Langmuir turbulence, the Stokes shear term in Eq. (1) is parameterized according to the literature (Li et al., 2016; Li and Fox-Kemper, 2017; Li et al., 2017), detailed in Section 2.3.

2.3 Parameterization of Langmuir Turbulence

Within the KPP (K-profile parameterization) scheme (Large et al., 1994), we implemented three recent Langmuir turbulence parameterizations (Van Roekel et al., 2012; Li et al., 2016; Li and Fox-Kemper, 2017; Li et al., 2017): (1) VR12-MA; (2)

https://doi.org/10.5194/egusphere-2022-1298
Preprint. Discussion started: 22 November 2022

LF17; (3) LF17-ST. Both VR12-MA and LF17 parameterize the Langmuir turbulence based on the waves: in VR12-MA the KPP turbulent velocity scale is multiplied by an enhancement factor based on the Langmuir turbulence; in LF17 the KPP turbulent velocity scale is treated in the same way as VR12-MA, and the entrainment buoyancy flux due to Langmuir turbulence is also considered. On the other hand, LF17-ST parameterizes the Langmuir turbulence similarly to LF17, but based on the 10-m winds instead of using the output from WW3.

For all the implemented schemes, the turbulent velocity scale w_s is modified by multiplying with an enhancement factor ε as:

$$w_s = \frac{\kappa u^*}{\phi}\varepsilon \tag{3}$$

where κ is the von Karman constant; u^* is the friction velocity; ϕ is the stability function defined by Large et al. (1994); the enhancement factor is defined as:

$$\varepsilon = |\cos(\alpha)|\sqrt{1+(1.5La_{SLP})^{-2}+(5.4La_{SLP})^{-2}}, \tag{4}$$

where α is the angle between wind and Langmuir cells; La_{SLP} is the Langmuir number (Van Roekel et al., 2012; Li et al., 2016, 2019). Here we used the projected Langmuir number defined in Eq. (6) of Li et al. (2019) that using the surface averaged Stokes velocity.

In VR12-MA the entrainment flux due to Langmuir turbulence is not considered, but in LF17 the entrainment flux is implemented by revising the definition of the bulk Richardson number as:

$$Ri_b(z) = \frac{(B_r - B(z))|z|}{|\boldsymbol{u}_r - \boldsymbol{u}(z)|^2 + V_{tL}^2(z)}, \tag{5}$$

where B_r and $\boldsymbol{u}_r$ are the buoyancy and velocity averaged in the surface layer; $B(z)$ and $\boldsymbol{u}(z)$ are the local buoyancy and local velocity; the turbulence shear term V_{tL}^2 is defined as:

$$V_{tL}^2(z) = \frac{C_v N(z) w_s(z)|z|}{Ri_c}\left[\frac{0.15w_*^3 + 0.17u_*^3(1+0.49La_{SL}^{-2})}{w_s(z)^3}\right]^{\frac{1}{2}}, \tag{6}$$

where dimensionless coefficient $C_v = \max(2.1 - 200\times\max(0,N), 1.7)$; $N(z)$ is the local buoyancy frequency; Ri_c is the critical Richardson number; La_{SL} is the Langmuir number defined in Eq. (5) of Li et al. (2019); $w_* = (-B_0/h)^{1/3}$ is the convective velocity scale; B_0 is the surface buoyancy flux; h is the KPP boundary layer depth.

In LF17-ST, the enhancement coefficient and entrainment flux are calculated similarly to LF17, but the Langmuir turbulence coefficient La is determined by the Stokes velocity parameterized from 10-m wind and mixed layer depth. The details can be found in Eq. (25) in Li et al. (2017). In this work, the implementations of LF17-ST in MITgcm followed the code provided by Schultz et al. (2020).

2.4 Wind Stress in MITgcm

The surface boundary condition is also modified by waves. The surface wind stress $\boldsymbol{\tau}_a$ is modified by subtracting the part that goes into wave growth $\boldsymbol{\tau}_{aw}$ and adding the wave-to-ocean momentum flux due to wave breaking $\boldsymbol{\tau}_{ow}$. Hence the ocean stress

https://doi.org/10.5194/egusphere-2022-1298
Preprint. Discussion started: 22 November 2022

is (Jenkins, 1989; Weber et al., 2006; Janssen, 2012):

$$\boldsymbol{\tau}_{oc} = \boldsymbol{\tau}_a - \boldsymbol{\tau}_{aw} + \boldsymbol{\tau}_{ow}, \tag{7}$$

where

$$\boldsymbol{\tau}_{aw} = \rho_w g \int_0^{2\pi}\int_0^{\infty} \frac{\boldsymbol{k}}{\omega} S_{in} \mathrm{d}\omega d\theta, \tag{8}$$

and

$$\boldsymbol{\tau}_{ow} = \rho_w g \int_0^{2\pi}\int_0^{\infty} \frac{\boldsymbol{k}}{\omega} S_{ds} \mathrm{d}\omega d\theta. \tag{9}$$

Here, S_{in} and S_{ds} are the wind input and wave dissipation source terms, respectively; $\boldsymbol{k}$ is the wave number; ω is the angular wave frequency; θ is the wave direction.

2.5 Ocean Roughness Closures

The parameterization of ocean roughness in WRF is also important. When WRF is not coupled to WW3, the bottom roughness is computed with the formulation proposed by Smith (1988), which is a combination of the formulae described by Liu et al. (1979) and Charnock (1955). When coupled with WW3 we parameterize the surface roughness based on the Charnock coefficient calculated from WW3 to make the surface roughness consistent. We have also implemented a few other ocean roughness closure models discussed in Olabarrieta et al. (2012): DGHQ (Drennan et al., 2003, which is based on wave age), TY2001 (Taylor and Yelland, 2001, which is based on wave steepness), and OOST (Oost et al., 2002, which considers both the effects of wave age and steepness). More detailed descriptions of these closure models and sensitivity analysis are presented in the appendix.

3 Experimental Design

3.1 Overview of the event

Cyclone Mekunu formed in the southeast Arabian Sea on May 20, 2018, and then propagated northwest before making landfall in southwest Oman on May 26. Categorized as ESCS (extremely severe cyclonic storm), cyclone Mekunu was the second cyclonic storm over the Arabian Sea in 2018 and the strongest tropical cyclone in the north Indian Ocean that year. The peak maximum sustained surface wind speed was 170-180 km/h gusting to 200 km/h (95 knots) and the lowest estimated central pressure was 960 hPa on May 25th (Government of India, 2018). Salalah, the capital city of southern Oman's Dhofar province, received 278.2 millimeters (10.95 inches) of rain in just 24 hours ending around 10:30 a.m. on May 26, over double the city's average annual rainfall of about five inches, with a total of 617 millimeters of rainfall during May 23-27 (Government of India, 2018). In addition to the extremely heavy rainfall in Oman and Yemen, cyclone Mekunu caused heavy rainfall that created

https://doi.org/10.5194/egusphere-2022-1298
Preprint. Discussion started: 22 November 2022

desert lakes over the “Empty Quarter” in Saudi Arabia. The warm, sandy, and wet soil was the perfect environment for the outbreak of desert locusts, posing a serious risk to food security and livelihoods (Salih et al., 2020).

3.2 Model Setups

To illustrate the coupled model capabilities, we perform the following types of model runs:

1. CPL.AOW: coupled ocean–wave–atmosphere (MITgcm–WW3–WRF) simulations.
2. CPL.AO: coupled ocean–atmosphere (MITgcm–WRF) simulations. The wave model is not coupled to the ocean or the atmosphere in the simulations, aiming to demonstrate the impact of the wave model on the simulation results.
3. ATM.DYN: stand-alone atmosphere (WRF) simulations. The wave model and the ocean model are not coupled to the atmosphere model. The SST forcing is from the HYCOM/NCODA $1/12°$ daily global analysis data (the Global Ocean Forecast System, Version 3.0 (Chassignet et al., 2007)). Compared with CPL.AO and CPL.AOW, this run serves as a benchmark that aims to demonstrate the impact of the ocean model on the simulation results.

The initial conditions, boundary conditions, and forcing terms of the simulations are outlined in Table 1. In the coupled runs, the ocean model uses the assimilated HYCOM/NCODA $1/12°$ daily global analysis data as initial and boundary conditions for ocean temperature, salinity, and horizontal velocities (Chassignet et al., 2007). The boundary conditions for the ocean are updated by linearly interpolating between the daily HYCOM/NCODA analysis data. A restoring layer with a width of 13 grid cells is applied at the lateral boundaries to enforce the boundary conditions. The inner and outer boundary relaxation timescales are 10 and 0.5 days, respectively. The atmosphere is initialized using the NCEP (National Centers for Environmental Prediction) FNL (Final) Operational Global Analysis data. The same data also provide the boundary conditions for air temperature, wind speed, and humidity. The atmospheric boundary conditions are updated based on linearly interpolating between 6-hourly NCEP FNL data. The ‘specified’ zone in WRF prescribes the lateral boundary values, and the ‘relaxation’ zone is used to nudge the solution from the domain interior toward the boundary condition value. Here we use the default width of one point for the specified zone and four points for the relaxation zone. In the wave model, the wave spectra at the offshore boundary come from the global wave modeling system described by Rascle and Ardhuin (2013). To initialize the wave model, we allowed the wave field to spin-up for 19 days from May 01, 2018 and then we analyze the period from May 20, 2018.

To generate the grids, we choose the latitude–longitude (cylindrical equidistant) map projection for MITgcm, WW3, and WRF. The model domain extends from 0 to 30.6°N and from 30°E to 78°E. The horizontal grid has 448×640 (lat$\times$long) cells and the spacing is 0.08° in both directions. We use identical horizontal grids for all model components to eliminate the complication of regridding winds near steep orography and complex coastlines, although the regridding capability is implemented in SKRIPS. There are 40 sigma layers in the atmosphere model (top pressure is 50 hPa) and 50 z-layers in the ocean model ($dz = 4$ m in the top). The wave model has a spectral grid of 48 directions (7.5° resolution) and 32 frequencies exponentially spaced from 0.0343 to 1.1 Hz.

Importantly, the coupled and uncoupled simulations derive skill from boundary conditions (i.e. they are dynamically downscaled hindcasts). This better allows us to focus on the impacts of air–sea interactions during the tropical cyclone event by minimizing the boundary errors. Because of the chaotic nature of the atmosphere, we generated 20-member ensembles for each run by adding small random perturbations to the initial SST (<0.01 °C) at every grid point in the coupled model.

The time step of the ocean model is 120 seconds. The horizontal sub-grid mixing is parameterized using nonlinear Smagorinsky viscosities, and the K-profile parameterization (KPP) is used for vertical mixing processes (Large et al., 1994) with modifications accounting for Langmuir mixing (Van Roekel et al., 2012; Li et al., 2016; Li and Fox-Kemper, 2017; Li et al., 2017). The time step of the atmosphere model is 30 seconds. The Morrison 2-moment scheme (Morrison et al., 2009) is used to resolve the microphysics; the updated version of the Kain–Fritsch convection scheme (Kain, 2004) is used for cumulus parameterization; the Mellor–Yamada–Nakanishi–Niino (MYNN) 2.5-order closure scheme (Nakanishi and Niino, 2004, 2009) is used for the planetary boundary layer (PBL); the Rapid Radiation Transfer Model for GCMs (RRTMG; (Iacono et al., 2008)) is used for longwave and shortwave radiation transfer through the atmosphere; the Noah land surface model is used for the land surface processes (Tewari et al., 2004). This selection of physics schemes is the same as in our previous work (Sun et al., 2021). The wave model uses a global integration time step of 600 s, spatial advection time step of 60 s, spectral advection time step of 60 s, and minimum source term time step of 10 s. The coupling interval is 120 seconds to allow for the capturing of the diurnal cycle of air–sea fluxes. In CPL.AOW we parameterized the Stokes shear in the same way as Li and Fox-Kemper (2017) by considering the effect of Langmuir turbulence. The Stokes–Coriolis and the Stokes–Advection in Eq. (1) are considered; the ocean surface roughness is determined using the Charnock coefficient (CHNK) calculated from WW3; the wind stress in the ocean model is treated as mentioned in Eq. (7).

3.3 Validation Data

To evaluate the performance of the simulations, the model outputs are compared with available data. The track of the tropical cyclone, the tropical central pressure, and the maximum wind speed are validated against IBTrACs data (Knapp et al., 2010, 2018). Here we use the IBTrACS–World Meteorological Organization version. IBTrACS provides a compilation of historical TC data as recorded by meteorological centers and/or forecast agencies and in this case the data from Indian Meteorological Department (IMD) are used.

The SST is validated by using in-situ observations from the satellite-tracked drifters of the Global Drifter Program (GDP, from https://www.aoml.noaa.gov/envids/gld/index.php) (Lumpkin and Pazos, 2007). The simulated SST fields are also validated against the $1/12°$ daily HYCOM/NCODA data. Because the HYCOM/NCODA analysis data are the initial and boundary conditions in the coupled model, this aims to show the error increase from the initial condition. We used bilinear interpolation to map the validation data onto the model grid to compare the results in a consistent way. When interpolating SST, only the values on ocean points are used.

4 Results

In this section, the ensemble coupled simulation results are compared with the results from the uncoupled runs to assess the performance of the coupled model and the impact of coupled feedbacks. We compared the ensemble-averaged characteristics

https://doi.org/10.5194/egusphere-2022-1298
Preprint. Discussion started: 22 November 2022

Table 1. The computational domain, WRF physics schemes, initial condition, boundary condition, and forcing terms used in the present simulations.

run	CPL.AOW and CPL.AO	ATM.DYN
model region	0 to 30.6°N; 30°E to 78°E	
horizontal resolution	408×640 (lat×long)	
grid spacing	0.075° × 0.075° (lat×long)	
microphysics scheme	Morrison 2-moment scheme	
convection scheme	Kain–Fritsch scheme	
PBL scheme	Mellor–Yamada–Nakanishi–Niino 2.5-order scheme	
longwave radiation scheme	Rapid Radiation Transfer Model for GCMs (RRTMG)	
shortwave radiation scheme	Rapid Radiation Transfer Model for GCMs (RRTMG)	
land surface scheme	Noah land surface model	
vertical levels	40 (atmosphere) 50 (ocean)	40 (atmosphere only)
initial and boundary conditions	NCEP FNL (atmosphere) HYCOM/NCODA (ocean)	NCEP FNL (atmosphere only)
ocean surface conditions	from MITgcm	HYCOM/NCODA
atmospheric forcings for ocean model	from WRF	not necessary

of the tropical cyclone (e.g., track, intensity, and wind speed), the changes in the ocean (e.g., sea surface temperature and mixed layer depth), and the waves generated by the tropical cyclone. By comparing the coupled run with uncoupled runs, we aim to (1) demonstrate the capability of the coupled model and (2) illustrate the impact of including ocean–wave–atmosphere interactions on simulating this tropical cyclone event.

4.1 Cyclone Track, Intensity, Wind Speed

First, we examine the characteristics of cyclone Mekunu obtained with and without coupling, aiming to demonstrate the capability of the coupled model. The tracks of the tropical cyclone, defined by the positions of the low pressure center, are presented in Fig. 2, where it can be seen that both models can qualitatively match the observed evolution and track. Although the translation speed of the tropical cyclone from CPL.AOW is somewhat slower (CPL.AOW: 236 km/day; IBTrACS: 254 km/day), the distances between the cyclone centers for all model runs and IBTrACS data are less than 250 km until May 26, shown in Fig. 3(a).

The characteristics of cyclone Mekunu (i.e., cyclone central pressure and maximum wind speed) obtained in the ensemble simulations are compared quantitatively with IBTrACS data in Fig. 3(b) and Fig. 3(c). From May 22 to May 27, the root-

https://doi.org/10.5194/egusphere-2022-1298
Preprint. Discussion started: 22 November 2022

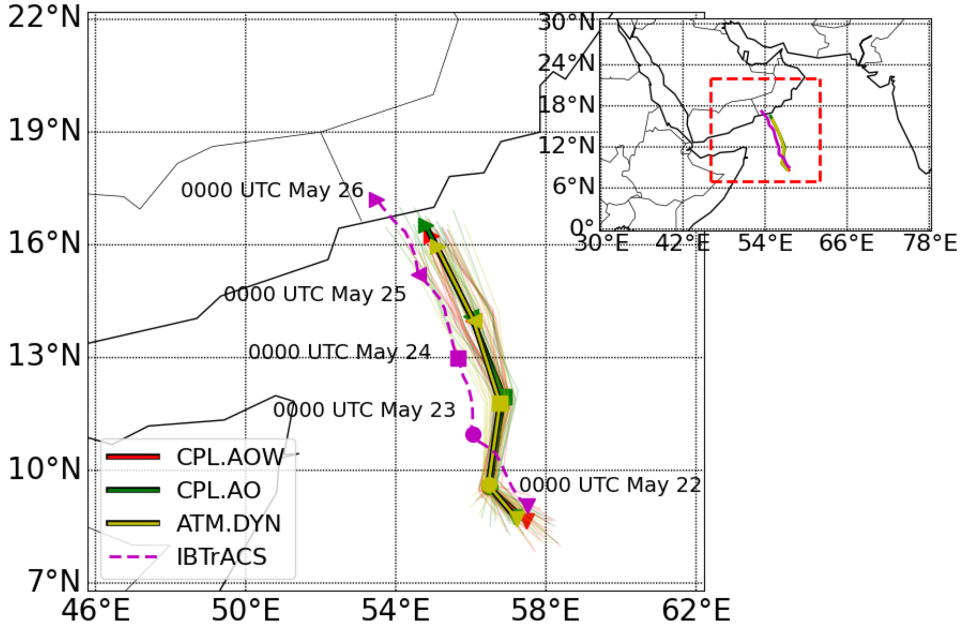

Figure 2. Comparison between the tracks of cyclone Mekunu obtained from IBTrACS data and the simulations. The thick solid lines indicate the tropical cyclone tracks obtained from averaging all ensemble members; the thin solid lines indicate the tropical cyclone tracks obtained from individual ensemble members. The text and markers highlight the time and locations of the cyclone at specific times.

mean-square-errors (RMSEs) of the cyclone low pressure center are 10.04, 9.36, and 10.25 hPa for CPL.AOW, CPL.AO, and ATM.DYN, respectively (ensemble standard deviations are 3.25, 3.14, and 2.92 hPa). The RMSEs of the maximum wind speed are 9.30, 8.63 and 9.76 m/s for CPL.AOW, CPL.AO, and ATM.DYN (ensemble standard deviations are 2.79, 2.73, and 2.72 m/s). In addition, the ensemble mean lowest pressures in CPL.AOW, CPL.AO, and ATM.DYN are higher than the IBTrACS data by 4.6, 5.4, and 17.7 hPa, respectively. The overestimation in ATM.DYN is more significant than one standard deviation between May 25 to 26. For the maximum wind speed, CPL.AOW and CPL.AO underestimate the maximum wind speed by about 5.9 m/s and 7.3 m/s, while in ATM.DYN the underestimation is as large as 13.5 m/s. The ATM.DYN does not capture the intensification of the TC between May 24 and 26 that is present in the IBTrACS observations and in the coupled simulations. We hypothesize that this is due to the SST cooling in ATM.DYN being greater than in the coupled simulations (see Section 4.2). Despite CPL.AOW better simulates the minimum pressure and maximum wind speed compared with the IBTrACS data than CPL.AO, the overall performance of CPL.AOW is not better but somewhat worse than CPL.AO, although both coupled runs better simulate the tropical cyclone than ATM.DYN.

To highlight the surface fluxes from the simulation, we show the snapshots of the wind speed and latent heat fluxes (LHFs) in Fig. 4. Instead of plotting the entire computational domain, we highlight the region around the center of the tropical cyclone (from 7°N to 22°N and from 46°E to 62°E). The 10-m wind speeds obtained in CPL.AOW and CPL.AO are generally consistent, except for the region near the center of the cyclone. Figure 4(c) shows a smaller area of high wind speeds (indicated by

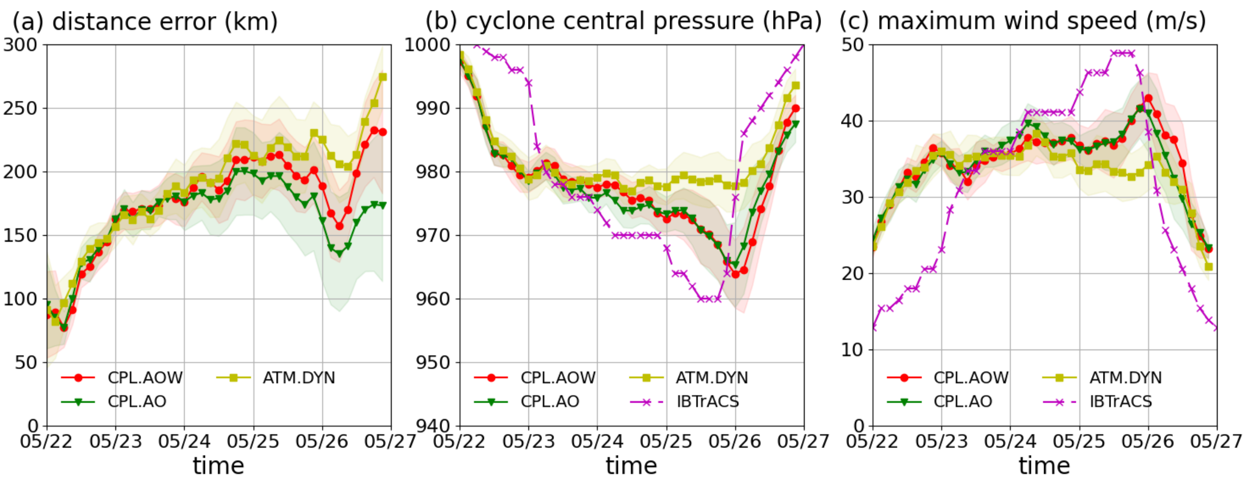

Figure 3. The characteristics of cyclone Mekunu obtained from the simulations plotted as functions of time. The solid lines indicate the ensemble averaged simulation results; the shaded areas indicate the standard deviation of the results. Panel (a) shows the distance errors in comparison with IBTrACS data; Panel (b) shows the cyclone central pressure; Panel (c) shows the maximum wind speed.

the contour of 15 m/s) in ATM.DYN because the uncoupled run underestimates the intensity of the cyclone. We highlighted the LHFs because they are the major component of the net surface heat fluxes and they are associated with the water vapor uptake. The LHFs are weak along the cyclone tracks due to the cold wake (shown in Fig. 5 in Section 4.2) but are generally consistent in CPL.AOW and CPL.AO, shown in Fig. 4(d-f). Near the center of the tropical cyclone in Fig. 4, the LHFs in ATM.DYN are weaker than the coupled runs by a few hundreds of W/m^2, and this is because the tropical cyclone is weaker due to cooler SST in ATM.DYN (the SST differences are detailed in Section 4.2). The largest differences in cyclone track, intensity, and wind speed are between the uncoupled (ATM.DYN) and coupled (CPL.AO, CPL.AOW simulations, with the latter being closer to IBTrACS observations.

4.2 SST and Mixed Layer Depth

The evolution of SST and ocean MLD from CPL.AOW and ATM.DYN is presented in Fig. 5 to highlight the impact of the tropical cyclone on the ocean. The results obtained from CPL.AO are not presented here, but in Section 5 we investigate the effect of wave coupling on the coupled system on SST and MLD. Figure 5(a) shows the differences of ensemble averaged SST between May 20 and May 27 (May 27 SST minus May 20 SST). This aims to highlight the development of an SST cold wake during this event. It can be seen that the SST cools down by a maximum of 4°C along the TC track, which can impact the ocean and air–sea interactions (Price, 1981; Stramma et al., 1986; Pasquero et al., 2021). The SST cooling in HYCOM shown in Fig. 5(b) is stronger than that in CPL.AOW. The stronger SST cooling in HYCOM SST is used to drive ATM.DYN and could impact the tropical cyclone intensity in the simulation results presented in Section 4.1. It should be noted that CPL.AOW also captures the SST warming in the Arabian Gulf and the Gulf of Aden.

https://doi.org/10.5194/egusphere-2022-1298
Preprint. Discussion started: 22 November 2022

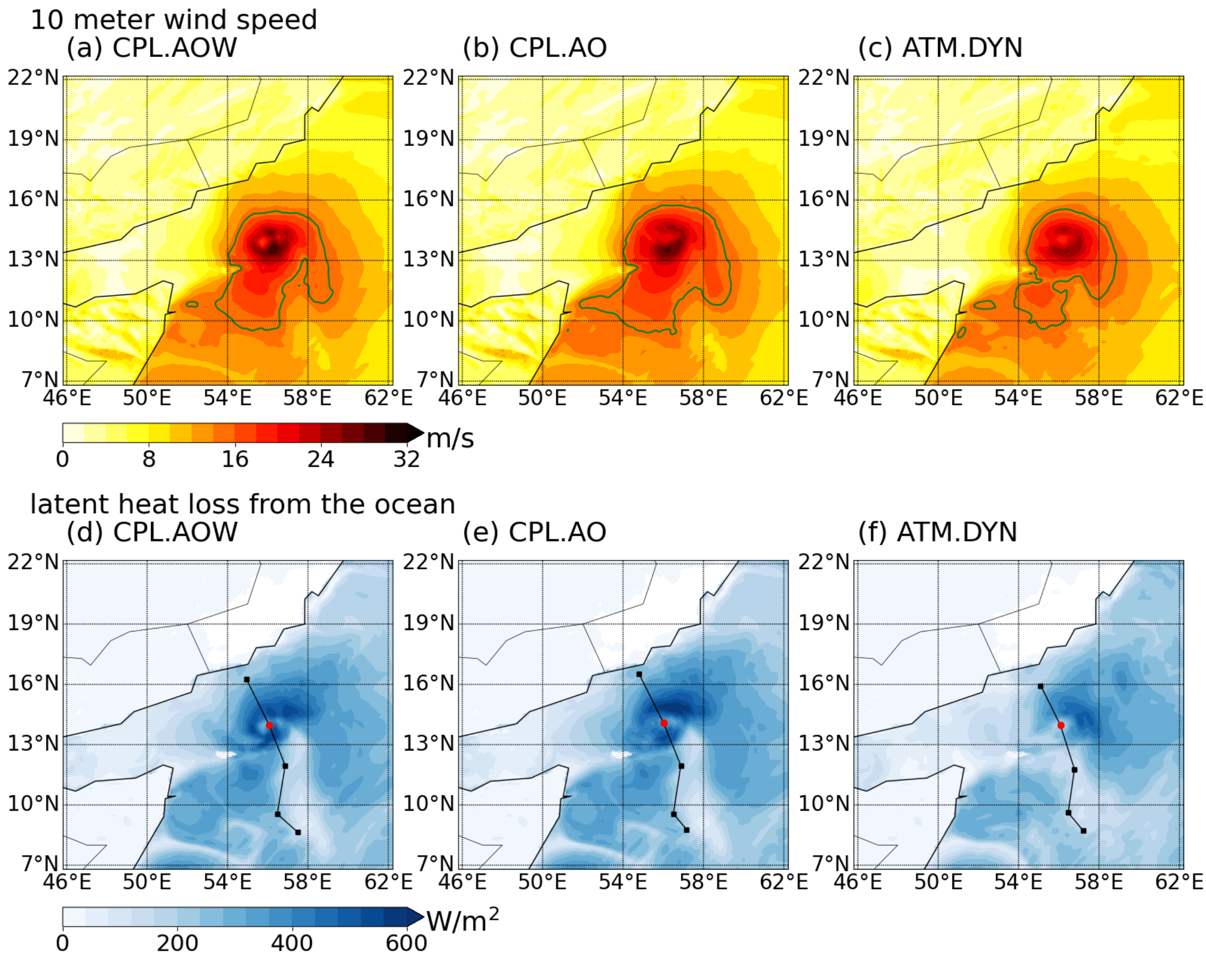

Figure 4. The snapshots of the wind speed and latent heat fluxes at 00 UTC May 25 obtained in the simulations. The ensemble averaged fields are plotted and we highlighted the region between 7°N to 22°N and from 46°E to 62°E. In Panels (a-c) the 15 m/s contour of the wind speed is used to highlight the size of the tropical cyclone. The black solid lines indicate the ensemble-averaged track of tropical cyclone in the simulations shown in Fig. 2.

The evolution of the mixed layer depth during the event is shown in Fig. 6 to demonstrate the impact of the tropical cyclone on ocean mixing. Here we are using $\Delta\rho = 0.03\ \mathrm{kg/m^3}$ to define the MLD. The initial MLD is about 30-40 meters along the track of the tropical cyclone. To highlight the evolution of the mixed layer, the differences of ensemble averaged MLD between May 20 and May 27 (May 27 MLD minus May 20 MLD) are plotted in Fig. 6(b). It can be seen that the MLD deepens by approximately 30-40 meters (the standard deviation is about 10 meters) along the track of the tropical cyclone, which is almost a 100% increase compared to its initial value in Fig. 6(a).

https://doi.org/10.5194/egusphere-2022-1298
Preprint. Discussion started: 22 November 2022

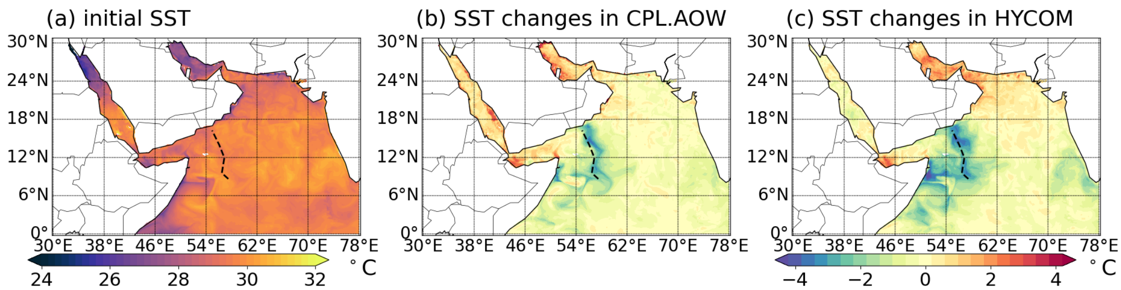

Figure 5. The evolution of SST during the tropical cyclone event. Panel (a) shows the SST when the simulation is initialized at 00 UTC May 20; Panel (b) illustrates the ensemble averaged SST changes between 00 UTC May 20 and 00 UTC May 27 in CPL; Panel (c) shows the SST changes in the HYCOM analysis for the same period.

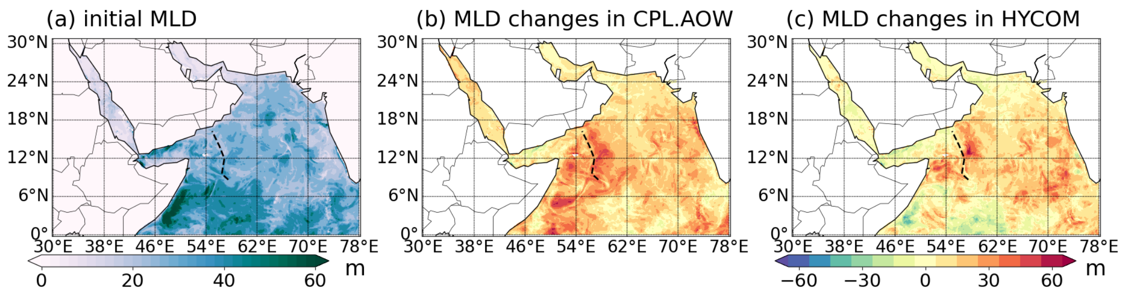

Figure 6. The evolution of MLD during the tropical cyclone event. Panel (a) shows the MLD at 00 UTC May 20 when the simulation is initialized; Panel (b) shows ensemble averaged MLD changes between 00 UTC May 20 and 00 UTC May 27 in CPL; Panel (c) shows the MLD changes in the HYCOM analysis for the same period.

4.3 Waves

Ocean surface waves are expected to affect air–sea interactions. The ensemble mean significant wave height (H_s) and the ensemble standard deviation obtained from the coupled simulation are shown in Fig. 7. The snapshot of the ensemble-averaged H_s at 00 UTC May 26 is presented in Fig. 7(a). The ensemble averaged H_s is as high as 8 m near the eye wall of the tropical cyclone. Figure 7(a) shows that alternating regions of high and low waves can be observed between 12°N to 24°N and from 60°E to 75°E. As discussed in Sun et al. (2022), this spatial pattern of high and low H_s is due to surface wave refraction by ocean currents.

Near the eye wall of the tropical cyclone, the standard deviation of H_s from the ensembles is approximately 3 m, showing that the wave height is sensitive to the wind speed (Fig. 7b), while the spatial variability of H_s, with alternating high and low beams, is consistent throughout the ensemble. Although CPL.AOW captures the overall spatial variability of H_s, the exact location of the beams deviates from the altimetry observations, since the central location of the tropical cyclone is not well captured by CPL.AOW. The comparison of the modeled H_s with altimeter data is shown in the appendix.

https://doi.org/10.5194/egusphere-2022-1298
Preprint. Discussion started: 22 November 2022

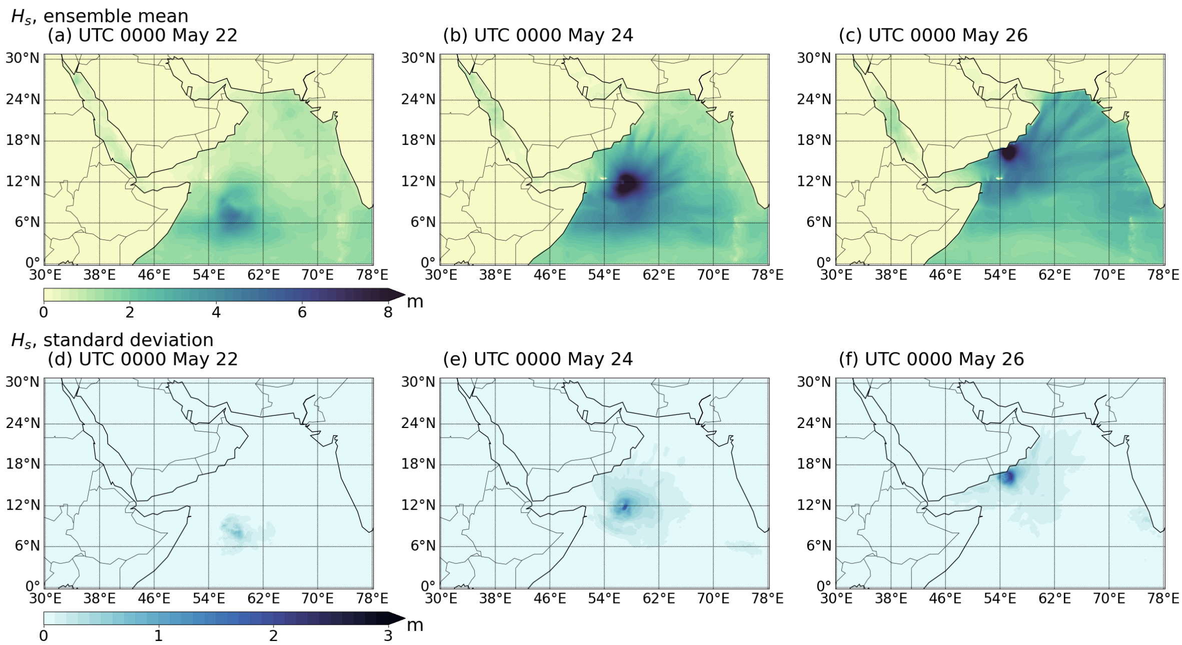

Figure 7. Snapshot of H_s at 00 UTC May 26, 2018. Panel (a) shows the ensemble averaged H_s obtained from CPL.AOW; Panel (b) shows the standard deviation of H_s of the ensembles from CPL.AOW.

5 Sensitivity Analysis to Wave Coupling

To explore the effects of the surface waves, coupled simulations were run using three recent parameterizations of Langmuir turbulence. We compared the characteristics of the tropical cyclone (e.g., track, intensity, and wind speed) and the changes in the ocean (e.g., SST and MLD). In the sensitivity analysis, we compare the simulation results without Langmuir turbulence (NoLT) and those with Langmuir turbulence (LF17, VR12-MA, and LF17-ST). This aims to illustrate the sensitivity of the coupled model to Langmuir turbulence, which may cool the SST and deepen the MLD during a tropical cyclone event. Note that the coupled run using LF17 is identical to CPL.AOW in Section 4. Because of the internal variability of the atmosphere model, we also performed the simulations using spectral nudging in WRF in addition to the "free runs" (simulations without spectral nudging). Although the simulations with spectral nudging have smaller internal variability, they underestimate the intensity of the tropical cyclone in the simulations.

Similar to the simulation results shown in Section 4, the characteristics of the cyclones are not significantly different from the simulations using different parameterizations. The cyclone characteristics in the sensitivity analysis are detailed in the Appendix. In this section we only highlight the sensitivity of SST, ocean mixed layer, and other surface fluxes to the parameterization of Langmuir turbulence.

https://doi.org/10.5194/egusphere-2022-1298
Preprint. Discussion started: 22 November 2022

5.1 SST and ocean mixed layer

To illustrate the impact of Langmuir turbulence on the upper ocean, a sensitivity analysis of the SST and the ocean mixed layer is performed. First we compare the SST cooling obtained in the simulations with the observational data from Global Drifter Program (Lumpkin and Centurioni, 2019). In Fig. 8 we show the SST changes throughout the event along the drifter tracks. It can be seen that a drifter closest to the track of the TC (highlighted in Fig. 8) recorded a cooling of 3.81°C, while the SST cooling in CPL.NoLT is only 2.25°C (standard deviation: 0.37°C), worse than the simulated results when the waves are coupled in CPL.LF17 (2.53°C; standard deviation: 0.37°C). To highlight the SST differences between the simulations, we plotted the SST differences between the runs with and without Langmuir turbulence in Figure 9, with regions of significant SST changes ($P < 0.05$) highlighted. It can be seen in the figure that in CPL.LF17 and CPL.LF17-ST the SST cooling near the tracks of the cyclone is stronger by about 0.5°C in comparison with CPL.NoLT due to the effect of Langmuir turbulence. When the spectral nudging is added to reduce the randomness of the atmosphere model, the cyclones within the ensemble simulations are more similar and thus the SST cooling is more significant. On the other hand, when using VR12-MA, we observed weaker SST cooling compared with the simulation without Langmuir turbulence. After we examine the vertical profiles of the ocean, we hypothesize that too much diffusion is added to the ocean current velocity when using VR12-MA in this case. The reduction of vertical gradient in ocean current velocity reduces the turbulent shear and the ocean mixing, and contributes to a weaker SST cooling. More details on the SST cooling are presented in Section 5.2.

The comparison between the MLDs obtained from the simulations is shown in Fig. 10. Again, we highlight the regions with significant MLD changes ($P < 0.05$) for both "free run" and those with spectral nudging. Due to Langmuir turbulence, in CPL.LF17 and CPL.LF17-ST the MLDs are deeper by a maximum of about 20 meters than that of CPL.NoLT. When using VR12-MA, the MLD is shallower again due to the reduction of turbulent shear from the parameterization of Langmuir turbulence in this case.

5.2 The Vertical Profiles

To investigate the SST warming and cooling in the wake zone, we have plotted the vertical profiles of the Richardson number and its components in Fig. 11. Here we averaged the quantities of interest in the region between 7°N to 13°N and from 54°E to 58°E because large SST and MLD changes are observed in this region. Due to the internal variability of the atmosphere, we only compare the simulation results with spectral nudging.

To highlight the changes in the vertical profiles, in Fig. 11(a-d) we plotted the domain-averaged Richardson number, buoyancy difference, vertical density gradient, and velocity, which are the largest terms in Eq. (5). The vertical profiles show the impacts of Langmuir turbulence. When VR12-MA is applied, the Langmuir enhancement factor added to the turbulent velocity scale in Eq. (3) is eventually used in the turbulent viscosity term in KPP (Large et al., 1994). This increase in turbulent viscosity reduces the vertical shear, as shown in Fig. 11(d). While VR12-MA changes this shear, the buoyancy and vertical density gradient terms in the Richardson number in Eq. (5) do not change significantly, shown in Fig. 11(b) and 11(c). Hence, when the horizontal shear velocity is reduced, the ocean mixing also reduces in VR12-MA and the SST cooling is less significant

https://doi.org/10.5194/egusphere-2022-1298
Preprint. Discussion started: 22 November 2022

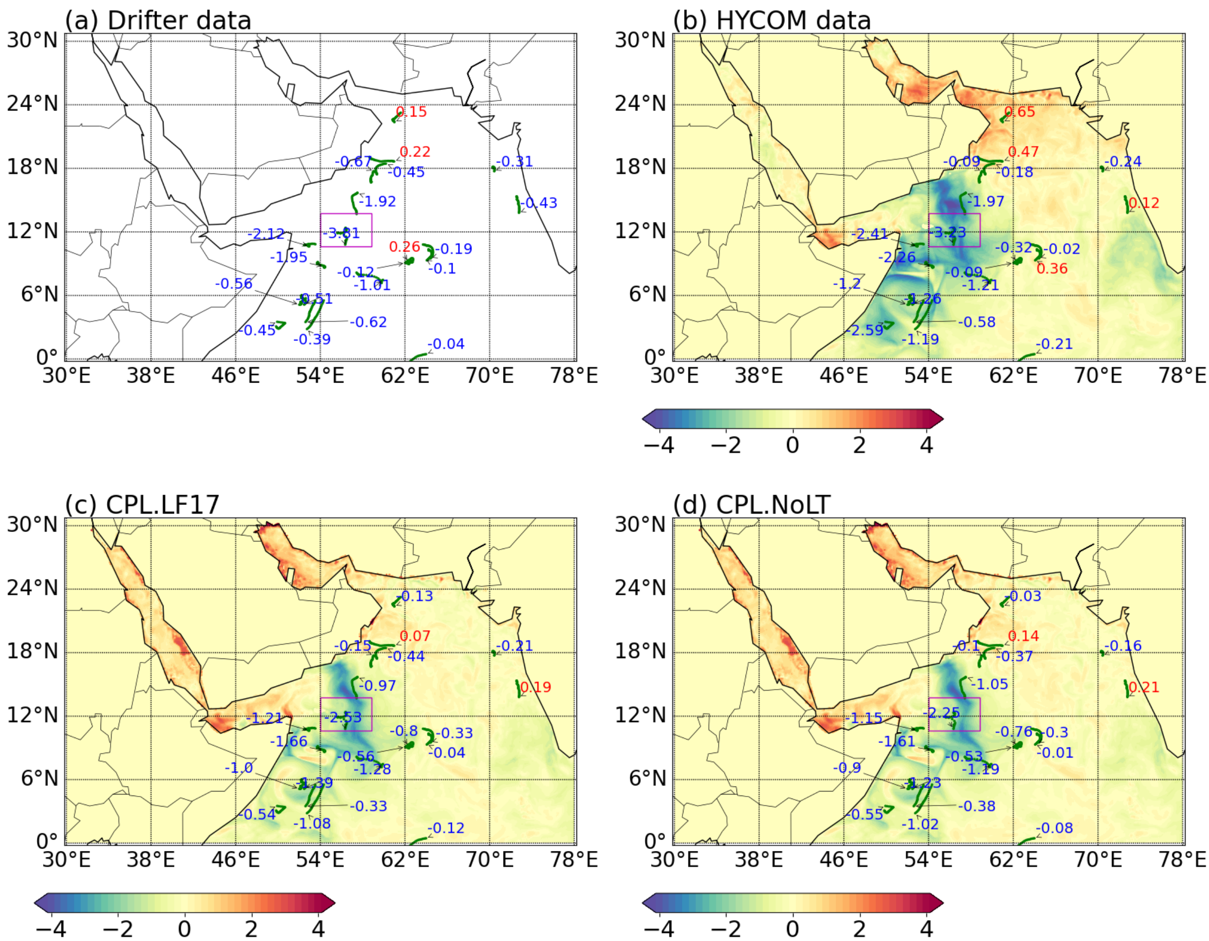

Figure 8. Evolution of the SST during the tropical cyclone event in comparison with drifter data. Panel (a) shows the SST changes during the event from drifter data; Panels (b-d) show the ensemble averaged SST changes from HYCOM, CPL.LF17, and CPL.NoLT, respectively. The red numbers indicate SST warming during the event; the blue numbers indicate SST cooling during the event.

than the simulation without Langmuir turbulence (NoLT). On the other hand, when LF17 is applied the Langmuir entrainment is considered when parameterizing the Richarson number. The effect of Langmuir entrainment induces stronger mixing by the tropical cyclone and deepens the mixing layer depth. Hence the SST cooling in the near wake region of the tropical cyclone is stronger when LF17 is used than VR12-MA.

6 Discussion and Summary

This work described the integration of WaveWatch III into the SKRIPS regional coupled model. The implementation allows using or not using the wave model in the SKRIPS model. The parameterizations of the surface waves are implemented in

https://doi.org/10.5194/egusphere-2022-1298
Preprint. Discussion started: 22 November 2022

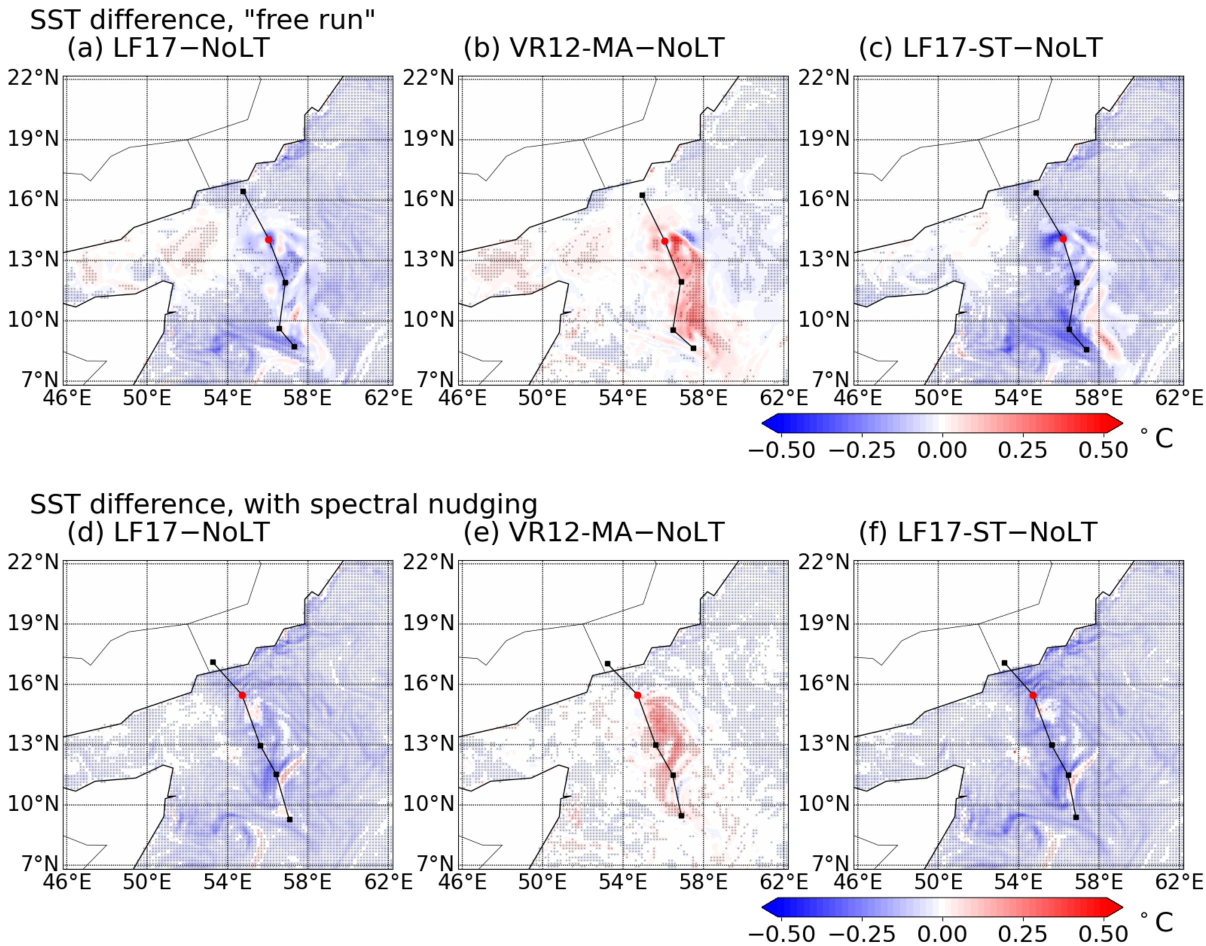

Figure 9. The snapshot of the ensemble averaged SST difference. Panels (a-c) show the SST difference between the simulations with Langmuir turbulence (CPL.LF17, CPL.VR12-MA, and CPL.LF17-ST) and without Langmuir turbulence (CPL.NoLT). Panels (d-f) show the same differences in the simulations with spectral nudging. The markers indicate the regions where the SST difference is significant ($P < 0.05$).

MITgcm to account for the impact of waves on the ocean as well as the Stokes–Advection and Stokes–Coriolis forces in the coupled model.

To test the coupled ocean–wave–atmosphere model, we performed a series of simulations of cyclone Mekunu in the Arabian Sea, which is a representative tropical cyclone case. In order to model the uncertainty due to the atmospheric internal variabilities, we added small perturbations to the initial SST to generate 20 ensembles for each test case. Then we compared the fully coupled simulations (CPL.AOW) with coupled runs without the wave model (CPL.AO) and stand-alone atmosphere simulations (ATM.DYN). The characteristics of the tropical cyclone (e.g., track, intensity, and wind speed) obtained in the two coupled simulations are similar within uncertainty. However, the stand-alone atmosphere model sees the SST cooling from the

https://doi.org/10.5194/egusphere-2022-1298
Preprint. Discussion started: 22 November 2022

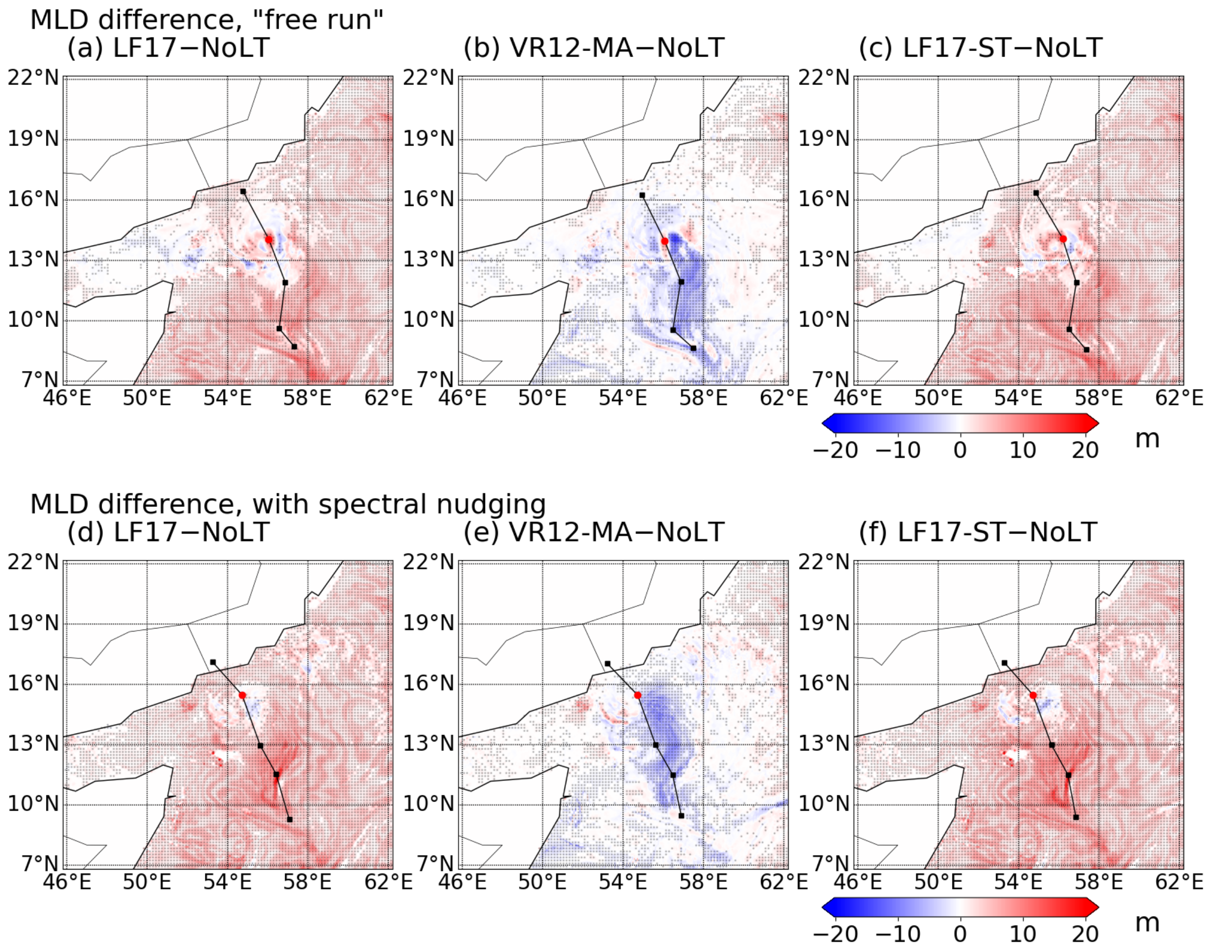

Figure 10. The snapshot of the ensemble averaged MLD difference. Panels (a-c) show the MLD difference between the simulations with Langmuir turbulence (CPL.LF17, CPL.VR12-MA, and CPL.LF17-ST) and without Langmuir turbulence (CPL.NoLT). Panels (d-f) show the same differences in the simulations with spectral nudging. The markers indicate the regions where the MLD difference is significant ($P < 0.05$).

HYCOM analysis that is stronger than in the coupled runs. Compared with the coupled simulations, in ATM.DYN the tropical cyclone has higher pressure and lower wind speed, making it less consistent with the observations.

We further tested the sensitivity of simulated characteristics of cyclone to wave coupling. The simulation results show that the characteristics of the tropical cyclone (e.g., intensity, pressure, maximum wind speed) are not sensitive to wave coupling compared with the internal variability of the model as resolved by the ensemble simulations. When the effect of Langmuir turbulence is parameterized using the LF17 and LF17-ST options that account for the Langmuir entrainment, the maximum SST cooling is about 0.5°C cooler and the maximum mixed layer deepening is about 20 m along the track of the tropical cyclone, indicating the surface waves play an important role in modulating the response of the upper ocean to tropical cyclone

https://doi.org/10.5194/egusphere-2022-1298
Preprint. Discussion started: 22 November 2022

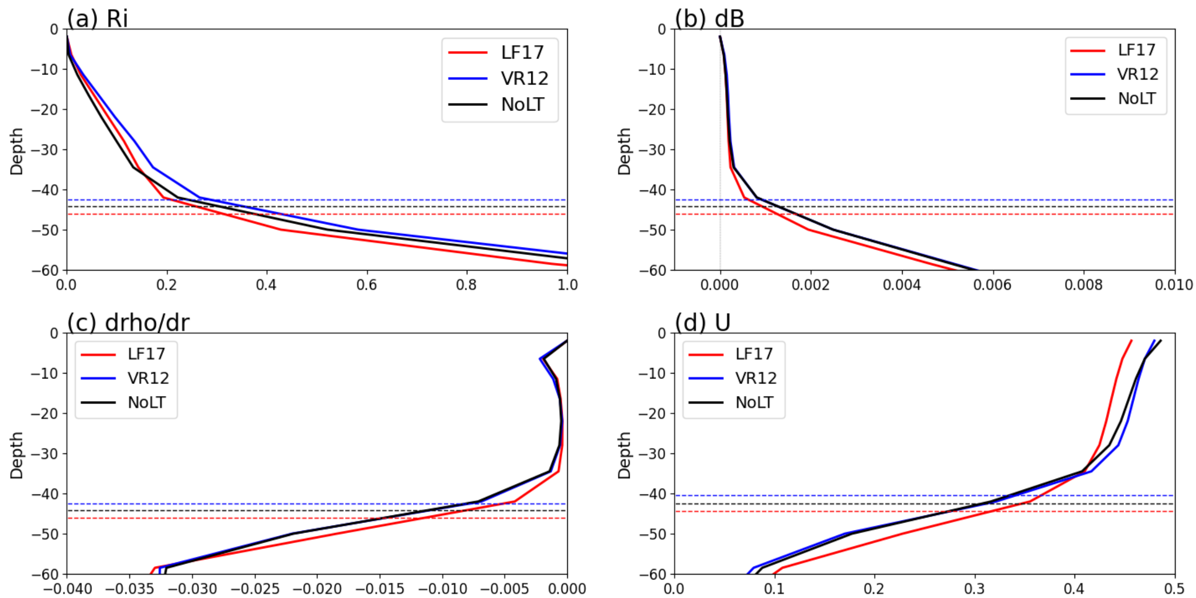

Figure 11. The snapshots of the vertical profiles at 00 UTC May 24 obtained in the simulations. Panel (a-d) show the Richardson number, buoyancy term, density changes, and horizontal velocity. The solid lines indicate the vertical profiles obtained from CPL.NoLT, CPL.VR12-MA, and CPL.LF17. The horizontal dashed lines indicate the mixed layer depth in MITgcm to illustrate the mixing layer.

surface forcing. On the other hand, when the effect of Langmuir turbulence is parameterized using the VR12-MA, the SST cooling and MLD deepening are weaker due to the changes of current shear in the coupled simulation.

The results presented here motivate further studies to evaluate and improve this and other regional or high resolution coupled models for investigating dynamical processes and forecasting applications, especially the interaction between ocean and waves and their feedback with the atmosphere.

Code availability. The source code of the coupled model is maintained on Github (https://github.com/iurnus/scripps_kaust_model) and Zenodo (https://doi.org/10.5281/zenodo.4014267). The code documentation is available at https://github.com/iurnus/scripps_kaust_model_doc

https://doi.org/10.5194/egusphere-2022-1298
Preprint. Discussion started: 22 November 2022

Appendix A: Ocean Roughness Closures

In this work, we implemented three different ocean roughness closure models in (Olabarrieta et al., 2012): (1) DGHQ model based on wave age (Drennan et al., 2003); (2) TY2001 model based on wave steepness (Taylor and Yelland, 2001); and (3) OOST model that considers both the effects of wave age and steepness (Oost et al., 2002). We also implemented another option that uses the Charnock coefficient (CHNK) calculated from WaveWatch III.

In Taylor and Yelland (2001), the ocean surface roughness is parameterized as:

$$\frac{z_0}{H_s} = 1200(H_s/L_p)^{4.5}, \tag{A1}$$

where z_0 is the ocean roughness; L_p is the wavelength at the peak of the wave spectrum; H_s is the significant wave height.

Drennan et al. (2003) proposed a wave age-based formula to characterize the ocean roughness. The wind friction velocity is also considered in this formula:

$$\frac{z_0}{H_s} = 3.35(u^*/C_p)^{3.4}, \tag{A2}$$

where u^* is the wind friction velocity; C_p is the wave phase speed at the peak frequency.

Oost et al. (2002) also derived the following expression for the ocean roughness based on the experimental data based on wave age and wavelength:

$$\frac{z_0}{L_p} = \frac{25}{\pi}(u^*/C_p)^{4.5}. \tag{A3}$$

Appendix B: Tropical Cyclone Characteristics Using Different Setups

The comparison between the simulations of cyclone Mekunu as resulting from the coupled models using different setups. Here we tested different setups in parameterizing Langmuir turbulence and sea surface roughness. For the Langmuir turbulence we test VR12-MA, LF17, LF17-ST, and no Langmuir turbulence; for the sea surface roughness we test CHAR, TY2001, DGHQ, and OOST, which is are all based on the wave output. The simulation using CHAR is the same as CPL.AOW in Section 4.

Figure A1 shows that the tracks of tropical cyclones from the coupled simulations are generally consistent within the ensemble spread, although the track from CPL is slightly closer to IBTrACS than the other simulations. The distance error, simulated cyclone central pressure, and maximum wind speed shown in Figs. A2 and A3 are also close. Note that the differences between the ensemble-mean pressure and wind speed in the coupled models are smaller than the standard deviations shown in Fig. A2 and Fig. A3. The snapshots of the 10-m wind speed and latent heat fluxes in Fig. A4 aim to illustrate the sensitivity of the surface atmosphere to parameterizing surface roughness. It can be seen that the 10-m wind speed is stronger and latent heat loss is also stronger when using TY2001, DGHQ, and OOST in comparison with using the CPL.AOW. However, the differences are not significant from the t-test (regions with $P < 0.05$ are highlighted).

https://doi.org/10.5194/egusphere-2022-1298
Preprint. Discussion started: 22 November 2022

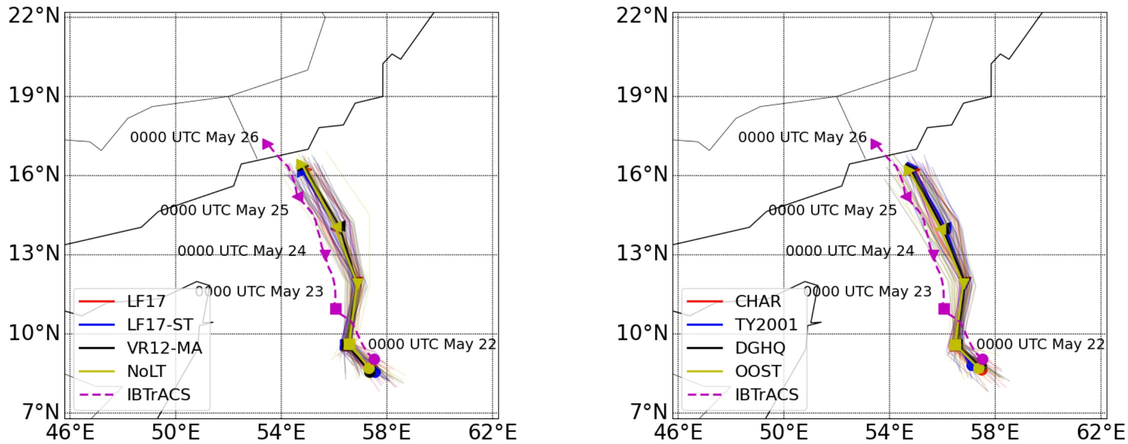

Figure A1. The tracks of cyclone Mekunu from the coupled simulations using different options to parameterize (a) Langmuir turbulence and (b) surface roughness. The thick solid lines indicate the locations of the center of the tropical cyclone obtained from averaging all ensemble members. The thin solid lines in the background denote the tracks of each ensemble member. The dashed lines denote the track of the tropical cyclone in IBTrACS data. The text and markers highlight the time and locations of the cyclone at specific times.

Appendix C: The significant wave height

To evaluate the simulation performance of surface waves, we compared the modeled H_s with along-track H_s measurements from the Jason-3 and SARAL/AltiKa altimeters. We use quality-controlled, unfiltered, and not resampled, along-track H_s measurements provided by the Institut Français de Recherche pour l'Exploitation de la MER (Queffeulou and Croizé-Fillon, 2013) (IFREMER; ftp://ftp.ifremer.fr/ifremer/cersat/products/swath/altimeters/waves/).

The comparison of the significant wave height H_s with the altimeter data is shown in Fig. A5. We also plotted the simulation results obtained in Sun et al. (2022). WAV.WND indicates the simulation using stand-alone WaveWatch III model driven by ERA5 wind only; WAV.CUR indicates the simulation using stand-alone WaveWatch III model driven by ERA5 wind and HYCOM currents. It can be seen from Fig. A5 that the coupled model captures the focusing and defocusing of the waves. However, because of the error in the location of the tropical cyclone, the patterns of the H_s are not completely consistent with the observational data.

Author contributions. RS worked on the coding tasks for integrating WW3 to the coupled system, wrote the code documentation, and performed the ensemble simulation. RS and AC drafted the initial manuscript. RS, ABVB, and SL implemented the WW3 wave model. All authors designed the computational framework and the numerical experiments. All authors discussed the results and contributed to the writing of the final manuscript.

https://doi.org/10.5194/egusphere-2022-1298
Preprint. Discussion started: 22 November 2022

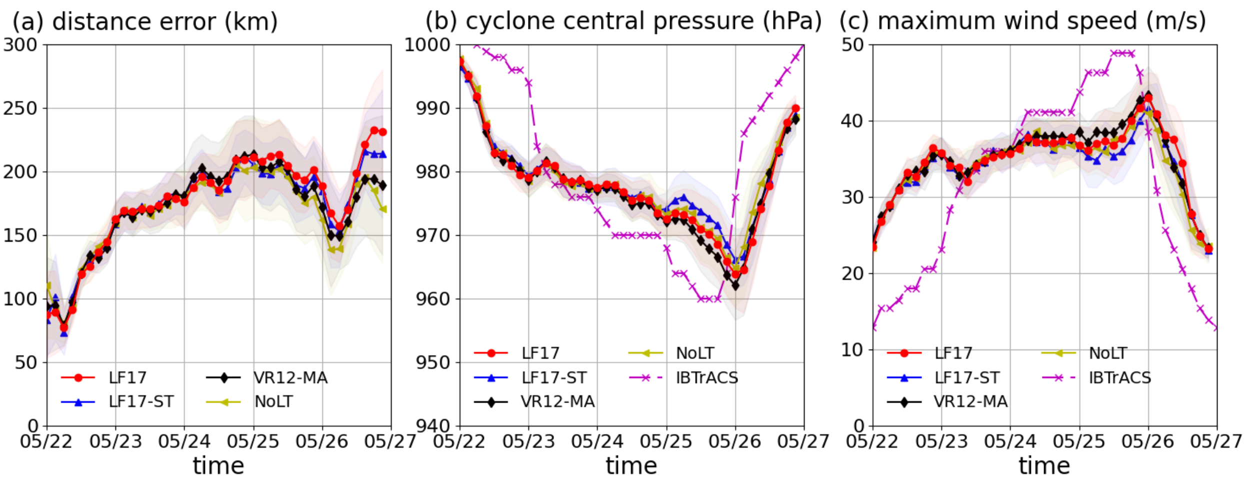

Figure A2. The characteristics of cyclone Mekunu obtained from the coupled simulations using different options to parameterize Langmuir turbulence. The solid lines indicate the ensemble averaged simulation results; the shaded areas indicate the standard deviation of the results. Panel (a) shows the distance errors in comparison with IBTrACS data; Panel (b) shows the cyclone central pressure; Panel (c) shows the maximum wind speed.

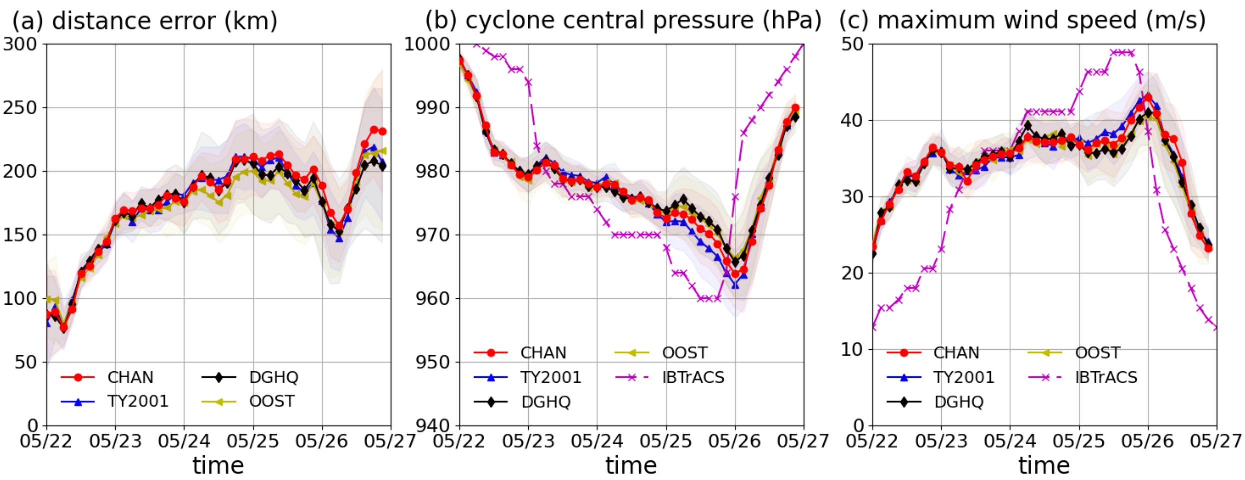

Figure A3. The characteristics of cyclone Mekunu obtained from the coupled simulations using different options to parameterize surface roughness. The solid lines indicate the ensemble averaged simulation results; the shaded areas indicate the standard deviation of the results. Panel (a) shows the distance errors in comparison with IBTrACS data; Panel (b) shows the cyclone central pressure; Panel (c) shows the maximum wind speed.

https://doi.org/10.5194/egusphere-2022-1298
Preprint. Discussion started: 22 November 2022

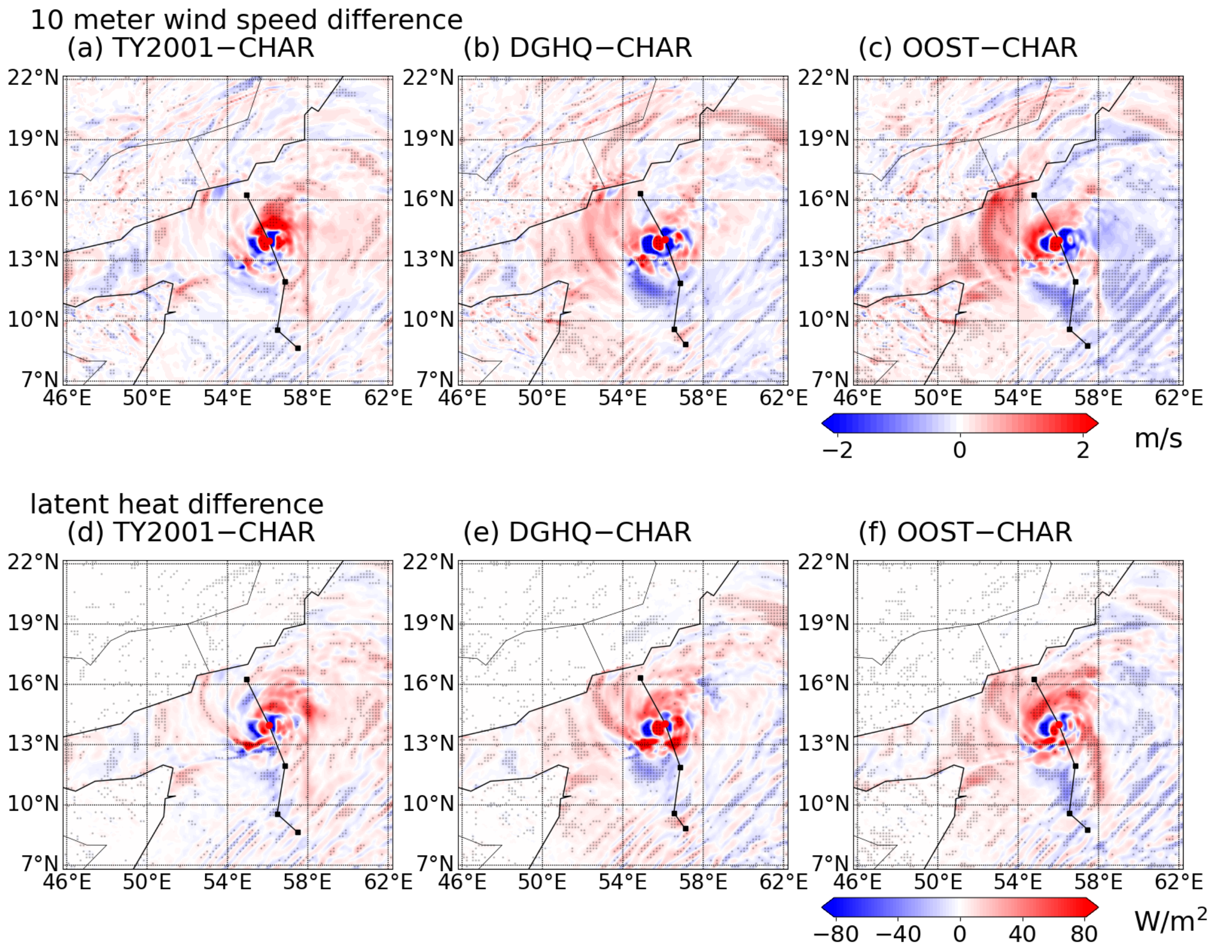

Figure A4. The snapshot of the ensemble averaged difference in 10-m wind speed and latent heat flux. Panels (a-c) show the 10-m wind speed difference between the simulations with different options to parameterize the surface roughness (TY2001, DGHQ, and OOST) and without paramerazations (CPL.CHAR). Panels (d-f) show the latent heat differences for the same simulations. The markers indicate the regions where the differences are significant ($P < 0.05$).

Competing interests. No competing interests are present.

Acknowledgements. We gratefully acknowledge the research funding (grant number: OSR-2016-RPP-3268.02) from KAUST (King Abdullah University of Science and Technology). We also appreciate the computational resources on supercomputer Shaheen II and the assistance provided by KAUST Supercomputer Laboratory. ABVB was supported by NASA award 80NSSC19K1004 through the S-MODE program. ACS was supported by NOAA Grant NA18OAR4310405 and ONR MISOBOB research initiative (N00014-17-S-B001). BDC and MRM were supported by NOAA Grant NA21OAR4310257, NA18OAR4310403, and NA22OAR4310597. AJM was partly supported by the Na-

https://doi.org/10.5194/egusphere-2022-1298
Preprint. Discussion started: 22 November 2022

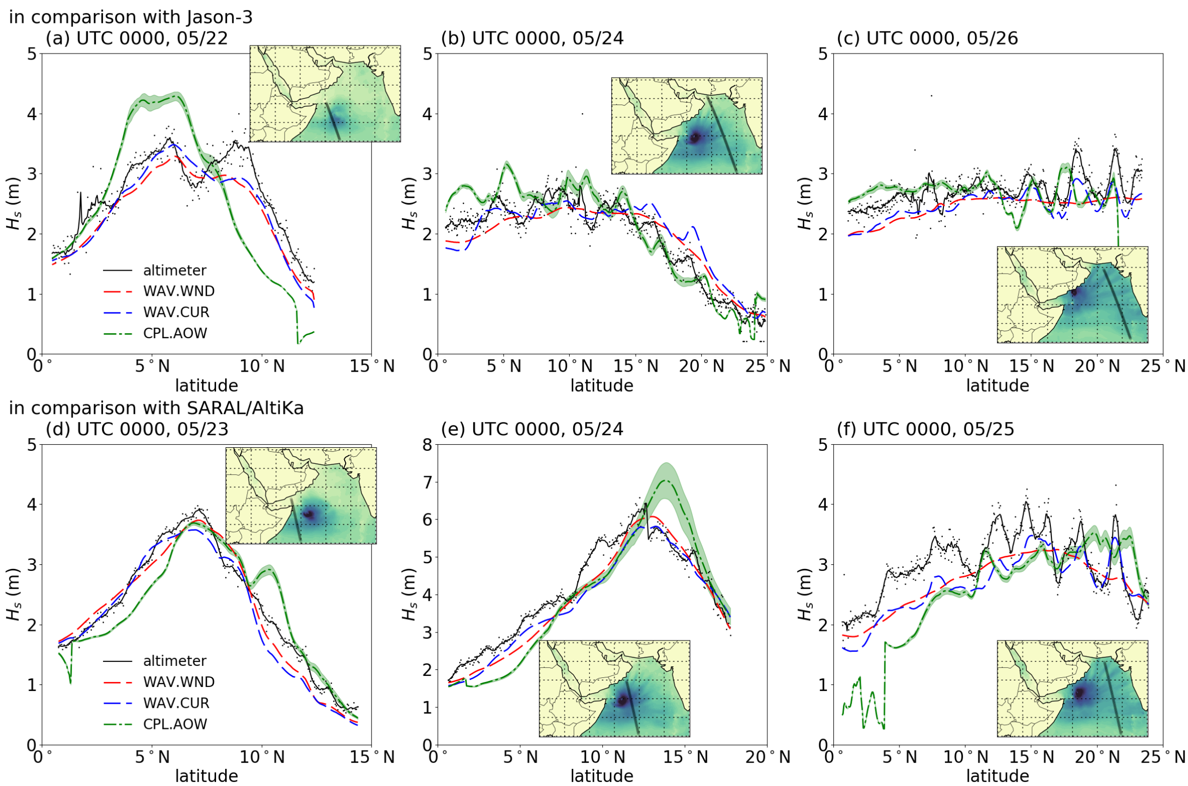

Figure A5. The ensemble averaged significant wave height in comparison with the altimeter data. Panels (a-c) show the comparison with Jason-3 data; Panels (d-f) show the comparison with SARAL data. The simulation results from Sun et al. (2022) are also presented. The shaded areas indicate the standard deviation of wave height in the ensemble simulations.

tional Science Foundation (OCE-2022868). We thank Baylor Fox-Kemper and Qing Li for discussing the implementation of the Langmuir
420 turbulence parameterizations.

https://doi.org/10.5194/egusphere-2022-1298
Preprint. Discussion started: 22 November 2022

References

Bender, M. A. and Ginis, I.: Real-case simulations of hurricane–ocean interaction using a high-resolution coupled model: Effects on hurricane intensity, Monthly Weather Review, 128, 917–946, 2000.

Bhatia, K., Vecchi, G., Murakami, H., Underwood, S., and Kossin, J.: Projected response of tropical cyclone intensity and intensification in a global climate model, Journal of Climate, 31, 8281–8303, 2018.

Blair, A., Ginis, I., Hara, T., and Ulhorn, E.: Impact of Langmuir turbulence on upper ocean response to Hurricane Edouard: Model and observations, Journal of Geophysical Research: Oceans, 122, 9712–9724, 2017.

Breivik, Ø., Janssen, P. A., and Bidlot, J.-R.: Approximate Stokes drift profiles in deep water, Journal of Physical Oceanography, 44, 2433–2445, 2014.

Campin, J.-M., Heimbach, P., Losch, M., Forget, G., edhill3, Adcroft, A., amolod, Menemenlis, D., dfer22, Hill, C., Jahn, O., Scott, J., stephdut, Mazloff, M., baylorfk, antnguyen13, Doddridge, E., Fenty, I., Bates, M., Martin, T., Abernathey, R., samarkhatiwala, Smith, T., Lauderdale, J., hongandyan, Deremble, B., raphael dussin, Bourgault, P., dngoldberg, and T., A. T.: MITgcm/MITgcm: checkpoint67m, https://doi.org/10.5281/zenodo.3492298, 2019.

Cerovečki, I., Sun, R., Bromwich, D. H., Zou, X., Mazloff, M. R., and Wang, S.-H.: Impact of downward longwave radiative deficits on Antarctic sea-ice extent predictability during the sea ice growth period, Environmental Research Letters, 17, 084 008, 2022.

Charnock, H.: Wind stress on a water surface, Quarterly Journal of the Royal Meteorological Society, 81, 639–640, 1955.

Chassignet, E. P., Hurlburt, H. E., Smedstad, O. M., Halliwell, G. R., Hogan, P. J., Wallcraft, A. J., Baraille, R., and Bleck, R.: The HYCOM (hybrid coordinate ocean model) data assimilative system, Journal of Marine Systems, 65, 60–83, 2007.

Chen, S. S., Price, J. F., Zhao, W., Donelan, M. A., and Walsh, E. J.: The CBLAST-Hurricane program and the next-generation fully coupled atmosphere–wave–ocean models for hurricane research and prediction, Bulletin of the American Meteorological Society, 88, 311–318, 2007a.

Chen, S. S., Price, J. F., Zhao, W., Donelan, M. A., and Walsh, E. J.: The CBLAST-Hurricane program and the next-generation fully coupled atmosphere–wave–ocean models for hurricane research and prediction, Bulletin of the American Meteorological Society, 88, 311–318, 2007b.

D'Asaro, E. A., Thomson, J., Shcherbina, A., Harcourt, R., Cronin, M., Hemer, M., and Fox-Kemper, B.: Quantifying upper ocean turbulence driven by surface waves, Geophysical Research Letters, 41, 102–107, 2014.

Drennan, W. M., Graber, H. C., Hauser, D., and Quentin, C.: On the wave age dependence of wind stress over pure wind seas, Journal of Geophysical Research: Oceans, 108, 2003.

Dube, S. K., Rao, A. D., Sinha, P. C., Murty, T. S., and Bahulayan, N.: Storm surge in the Bay of Bengal and Arabian Sea the problem and its prediction, Mausam, 48, 283–304, 1997.

Emanuel, K. A.: The theory of hurricanes, Annual Review of Fluid Mechanics, 23, 179–196, 1991.

Evan, A. T. and Camargo, S. J.: A climatology of Arabian Sea cyclonic storms, Journal of Climate, 24, 140–158, 2011.

Evan, A. T., Kossin, J. P., and Ramanathan, V.: Arabian Sea tropical cyclones intensified by emissions of black carbon and other aerosols, Nature, 479, 94–97, 2011.

Fairall, C., Bradley, E. F., Hare, J., Grachev, A., and Edson, J.: Bulk parameterization of air–sea fluxes: Updates and verification for the COARE algorithm, Journal of Climate, 16, 571–591, 2003.

https://doi.org/10.5194/egusphere-2022-1298
Preprint. Discussion started: 22 November 2022

Fan, Y., Ginis, I., and Hara, T.: The effect of wind–wave–current interaction on air–sea momentum fluxes and ocean response in tropical cyclones, Journal of Physical Oceanography, 39, 1019–1034, 2009.

Government of India, Ministry of Earth Sciences, I. M. D.: Extremely severe cyclonic storm, "MEKUNU" over the Arabian Sea (21–27 May 2018): A report., Tech. rep., New Delhi: India Meteorological Department. Retrieved from http://www.rsmcnewdelhi.imd.gov.in/index.php?option=com_content&view=article&id=198:preliminary-report-2018&catid=12:publications&Itemid=540&lang=en, 2018.

Henderson-Sellers, A., Zhang, H., Berz, G., Emanuel, K., Gray, W., Landsea, C., Holland, G., Lighthill, J., Shieh, S.-L., Webster, P., et al.: Tropical cyclones and global climate change: A post-IPCC assessment, Bulletin of the American Meteorological Society, 79, 19–38, 1998.

Hill, C., DeLuca, C., Balaji, Suarez, M., and Silva, A.: The architecture of the earth system modeling framework, Computing in Science & Engineering, 6, 18–28, 2004.

Iacono, M. J., Delamere, J. S., Mlawer, E. J., Shephard, M. W., Clough, S. A., and Collins, W. D.: Radiative forcing by long-lived greenhouse gases: Calculations with the AER radiative transfer models, Journal of Geophysical Research: Atmospheres, 113, 2008.

Janssen, P. A.: Ocean wave effects on the daily cycle in SST, Journal of Geophysical Research: Oceans, 117, 2012.

Jenkins, A. D.: The use of a wave prediction model for driving a near-surface current model, Deutsche Hydrografische Zeitschrift, 42, 133–149, 1989.

Kain, J. S.: The Kain–Fritsch convective parameterization: an update, Journal of Applied Meteorology, 43, 170–181, 2004.

Knapp, K. R., Kruk, M. C., Levinson, D. H., Diamond, H. J., and Neumann, C. J.: The international best track archive for climate stewardship (IBTrACS) unifying tropical cyclone data, Bulletin of the American Meteorological Society, 91, 363–376, 2010.

Knapp, K. R., Diamond, H. J., Kossin, J. P., Kruk, M. C., and Schreck, C. J.: The international best track archive for climate stewardship (IBTrACS) unifying tropical cyclone data, version 4, Tech. rep., [NI - North Indian]. NOAA National Centers for Environmental Information. https://doi.org/10.25921/82ty-9e16 [access date: Dec 01 2021]., 2018.

Langmuir, I.: Surface motion of water induced by wind, Science, 87, 119–123, 1938.

Large, W. G., McWilliams, J. C., and Doney, S. C.: Oceanic vertical mixing: A review and a model with a nonlocal boundary layer parameterization, Reviews of Geophysics, 32, 363–403, 1994.

Lewis, H. W., Castillo Sanchez, J. M., Arnold, A., Fallmann, J., Saulter, A., Graham, J., Bush, M., Siddorn, J., Palmer, T., Lock, A., et al.: The UKC3 regional coupled environmental prediction system, Geoscientific Model Development, 12, 2357–2400, 2019.

Li, Q. and Fox-Kemper, B.: Assessing the effects of Langmuir turbulence on the entrainment buoyancy flux in the ocean surface boundary layer, Journal of Physical Oceanography, 47, 2863–2886, 2017.

Li, Q., Webb, A., Fox-Kemper, B., Craig, A., Danabasoglu, G., Large, W. G., and Vertenstein, M.: Langmuir mixing effects on global climate: WAVEWATCH III in CESM, Ocean Modelling, 103, 145–160, 2016.

Li, Q., Fox-Kemper, B., Breivik, Ø., and Webb, A.: Statistical models of global Langmuir mixing, Ocean Modelling, 113, 95–114, 2017.

Li, Q., Reichl, B. G., Fox-Kemper, B., Adcroft, A. J., Belcher, S. E., Danabasoglu, G., Grant, A. L., Griffies, S. M., Hallberg, R., Hara, T., et al.: Comparing ocean surface boundary vertical mixing schemes including Langmuir turbulence, Journal of Advances in Modeling Earth Systems, 11, 3545–3592, 2019.

Li, Z., Tam, C.-Y., Li, Y., Lau, N.-C., Chen, J., Chan, S., Lau, D.-S. D., and Huang, Y.: How does air-sea wave interaction affect tropical cyclone intensity? An atmosphere–wave–ocean coupled model study based on super typhoon Mangkhut (2018), Earth and Space Science, 9, 2022.

Liu, B., Liu, H., Xie, L., Guan, C., and Zhao, D.: A coupled atmosphere–wave–ocean modeling system: Simulation of the intensity of an idealized tropical cyclone, Monthly Weather Review, 139, 132–152, 2011.

https://doi.org/10.5194/egusphere-2022-1298
Preprint. Discussion started: 22 November 2022

Liu, W., Katsaros, K., and Businger, J.: Bulk parameterization of air-sea exchanges of heat and water vapor including the molecular constraints at the interface, Journal of Atmospheric sciences, 36, 1722–1735, 1979.

Lumpkin, R. and Centurioni, L.: Global Drifter Program quality-controlled 6-hour interpolated data from ocean surface drifting buoys., Tech. rep., NOAA National Centers for Environmental Information. Dataset. https://doi.org/10.25921/7ntx-z961. Accessed Mar 01, 2022., 2019.

Lumpkin, R. and Pazos, M.: Measuring surface currents with Surface Velocity Program drifters: the instrument, its data, and some recent results, Lagrangian analysis and prediction of coastal and ocean dynamics, 39, 67, 2007.

Marshall, J., Adcroft, A., Hill, C., Perelman, L., and Heisey, C.: A finite-volume, incompressible Navier Stokes model for studies of the ocean on parallel computers, Journal of Geophysical Research: Oceans, 102, 5753–5766, 1997.

McWilliams, J. C., Sullivan, P. P., and Moeng, C.-H.: Langmuir turbulence in the ocean, Journal of Fluid Mechanics, 334, 1–30, 1997.

Mogensen, K. S., Magnusson, L., and Bidlot, J.-R.: Tropical cyclone sensitivity to ocean coupling in the ECMWF coupled model, Journal of Geophysical Research: Oceans, 122, 4392–4412, 2017.

Morrison, H., Thompson, G., and Tatarskii, V.: Impact of cloud microphysics on the development of trailing stratiform precipitation in a simulated squall line: Comparison of one-and two-moment schemes, Monthly Weather Review, 137, 991–1007, 2009.

Murakami, H., Vecchi, G. A., and Underwood, S.: Increasing frequency of extremely severe cyclonic storms over the Arabian Sea, Nature Climate Change, 7, 885–889, 2017.

Nakanishi, M. and Niino, H.: An improved Mellor–Yamada level-3 model with condensation physics: Its design and verification, Boundary-Layer Meteorology, 112, 1–31, 2004.

Nakanishi, M. and Niino, H.: Development of an improved turbulence closure model for the atmospheric boundary layer, Journal of the Meteorological Society of Japan. Ser. II, 87, 895–912, 2009.

Olabarrieta, M., Warner, J. C., Armstrong, B., Zambon, J. B., and He, R.: Ocean–atmosphere dynamics during Hurricane Ida and Nor'Ida: an application of the coupled ocean–atmosphere–wave–sediment transport (COAWST) modeling system, Ocean Modelling, 43, 112–137, 2012.

Oost, W., Komen, G., Jacobs, C., and Van Oort, C.: New evidence for a relation between wind stress and wave age from measurements during ASGAMAGE, Boundary-Layer Meteorology, 103, 409–438, 2002.

Pasquero, C., Desbiolles, F., and Meroni, A. N.: Air-sea interactions in the cold wakes of tropical cyclones, Geophysical Research Letters, 48, e2020GL091 185, 2021.

Price, J. F.: Upper ocean response to a hurricane, Journal of Physical Oceanography, 11, 153–175, 1981.

Queffeulou, P. and Croizé-Fillon, D.: Global altimeter SWH data set, version 10., Tech. rep., Laboratoire d'Océanographie Spatiale, IFREMER, Plouzané, France. Available at ftp://ftp.ifremer.fr/ifremer/cersat/products/swath/altimeters/waves/, 2013.

Rabe, T. J., Kukulka, T., Ginis, I., Hara, T., Reichl, B. G., D'Asaro, E. A., Harcourt, R. R., and Sullivan, P. P.: Langmuir turbulence under hurricane Gustav (2008), Journal of Physical Oceanography, 45, 657–677, 2015.

Rascle, N. and Ardhuin, F.: A global wave parameter database for geophysical applications. Part 2: Model validation with improved source term parameterization, Ocean Modelling, 70, 174–188, 2013.

Reichl, B. G., Ginis, I., Hara, T., Thomas, B., Kukulka, T., and Wang, D.: Impact of sea-state-dependent Langmuir turbulence on the ocean response to a tropical cyclone, Monthly Weather Review, 144, 4569–4590, 2016a.

Reichl, B. G., Wang, D., Hara, T., Ginis, I., and Kukulka, T.: Langmuir turbulence parameterization in tropical cyclone conditions, Journal of Physical Oceanography, 46, 863–886, 2016b.

https://doi.org/10.5194/egusphere-2022-1298
Preprint. Discussion started: 22 November 2022

Salih, A. A., Baraibar, M., Mwangi, K. K., and Artan, G.: Climate change and locust outbreak in East Africa, Nature Climate Change, 10, 584–585, 2020.

Sauvage, C., Seo, H., Clayson, C. A., and Edson, J. B.: Impacts of waves and sea states on air-sea momentum flux in the Northwest Tropical Atlantic Ocean: parameterization and wave coupled climate modeling, Earth and Space Science Open Archive, p. 30, https://doi.org/10.1002/essoar.10512415.1, 2022.

Saxby, J., Crook, J., Peatman, S., Birch, C., Schwendike, J., Valdivieso da Costa, M., Castillo Sanchez, J. M., Holloway, C., Klingaman, N. P., Mitra, A., et al.: Simulations of Bay of Bengal tropical cyclones in a regional convection-permitting atmosphere–ocean coupled model, Weather and Climate Dynamics Discussions, pp. 1–40, 2021.

Schultz, C., Doney, S. C., Zhang, W. G., Regan, H., Holland, P., Meredith, M., and Stammerjohn, S.: Modeling of the influence of sea ice cycle and Langmuir circulation on the upper ocean mixed layer depth and freshwater distribution at the West Antarctic Peninsula, Journal of Geophysical Research: Oceans, 125, e2020JC016 109, 2020.

Skamarock, W. C., Klemp, J. B., Dudhia, J., Gill, D. O., Liu, Z., Berner, J., Wang, W., Powers, J. G., Duda, M. G., Barker, D. M., and Huang, X.-Y.: A description of the Advanced Research WRF Version 4, Tech. rep., NCAR Technical Note: NCAR/TN-556+STR, 145 pp, doi:10.5065/1dfh-6p97, 2019.

Smith, S. D.: Coefficients for sea surface wind stress, heat flux, and wind profiles as a function of wind speed and temperature, Journal of Geophysical Research: Oceans, 93, 15 467–15 472, 1988.

Stramma, L., Cornillon, P., and Price, J. F.: Satellite observations of sea surface cooling by hurricanes, Journal of Geophysical Research: Oceans, 91, 5031–5035, 1986.

Sun, R., Subramanian, A. C., Miller, A. J., Mazloff, M. R., Hoteit, I., and Cornuelle, B. D.: SKRIPS v1.0: a regional coupled ocean–atmosphere modeling framework (MITgcm–WRF) using ESMF/NUOPC, description and preliminary results for the Red Sea, Geoscientific Model Development, 12, 4221–4244, https://doi.org/10.5194/gmd-12-4221-2019, 2019.

Sun, R., Subramanian, A. C., Cornuelle, B. D., Mazloff, M. R., Miller, A. J., Ralph, F. M., Seo, H., and Hoteit, I.: The role of air–sea interactions in atmospheric rivers: Case studies using the SKRIPS regional coupled model, Journal of Geophysical Research: Atmospheres, 126, e2020JD032 885, 2021.

Sun, R., Villas Bôas, A. B., Subramanian, A. C., Cornuelle, B. D., Mazloff, M. R., Miller, A. J., Langodan, S., and Hoteit, I.: Focusing and defocusing of tropical cyclone generated waves by ocean current refraction, Journal of Geophysical Research: Oceans, p. e2021JC018112, 2022.

Suzuki, N. and Fox-Kemper, B.: Understanding Stokes forces in the wave-averaged equations, Journal of Geophysical Research: Oceans, 121, 3579–3596, 2016.

Taylor, P. K. and Yelland, M. J.: The dependence of sea surface roughness on the height and steepness of the waves, Journal of physical oceanography, 31, 572–590, 2001.

Tewari, M., Chen, F., Wang, W., Dudhia, J., LeMone, M., Mitchell, K., Ek, M., Gayno, G., Wegiel, J., and Cuenca, R.: Implementation and verification of the unified NOAH land surface model in the WRF model, in: 20th conference on weather analysis and forecasting/16th conference on numerical weather prediction, vol. 1115, American Meteorological Society Seattle, WA, 2004.

Thorpe, S.: Langmuir circulation, Annu. Rev. Fluid Mech., 36, 55–79, 2004.

Tolman, H. L.: A third-generation model for wind waves on slowly varying, unsteady, and inhomogeneous depths and currents, Journal of Physical Oceanography, 21, 782–797, 1991.

https://doi.org/10.5194/egusphere-2022-1298
Preprint. Discussion started: 22 November 2022

Van Roekel, L., Fox-Kemper, B., Sullivan, P., Hamlington, P., and Haney, S.: The form and orientation of Langmuir cells for misaligned winds and waves, Journal of Geophysical Research: Oceans, 117, 2012.

Warner, J. C., Armstrong, B., He, R., and Zambon, J. B.: Development of a coupled ocean–atmosphere–wave–sediment transport (COAWST) modeling system, Ocean Modelling, 35, 230–244, 2010.

Weber, J. E. H., Broström, G., and Saetra, Ø.: Eulerian versus Lagrangian approaches to the wave-induced transport in the upper ocean, Journal of Physical oceanography, 36, 2106–2118, 2006.

Wu, L., Breivik, Ø., and Rutgersson, A.: Ocean-wave-atmosphere interaction processes in a fully coupled modeling system, Journal of Advances in Modeling Earth Systems, 11, 3852–3874, 2019.

WW3DG: User Manual and System Documentation of WAVEWATCH III® Version 6.07, Tech. rep., WAVEWATCH III® Development Group, NOAA/NWS/NCEP/MMA College Park, MD, 2019.